

NMDAR-mediated transcriptional control of gene expression in the specification of interneuron subtype identity

Vivek Mahadevan^a, Apratim Mitra^b, Yajun Zhang^c, Areg Peltekian^a, Ramesh Chittajallu^a, Carola Esnault^{b,1}, Dragan Maric^d, Christopher Rhodes^c, Kenneth A. Pelkey^a, Ryan Dale^b, Timothy J. Petros^c, Chris J. McBain^{a,*}

^aSection on Cellular and Synaptic Physiology, Eunice Kennedy Shriver National Institute of Child Health and Human Development (NICHD), Bethesda, 20892, MD, USA

^bBioinformatics and Scientific Programming Core, NICHD, Bethesda, 20892, MD, USA

^cUnit on Cellular and Molecular Neurodevelopment, NICHD, Bethesda, 20892, MD, USA

^dFlow and Imaging Cytometry Core Facility, National Institute of Neurological Disorders and Stroke (NINDS), Bethesda, 20852, MD, USA

Abstract

Medial ganglionic eminence (MGE)-derived parvalbumin (PV)⁺, somatostatin (SST)⁺ and Neurogliaform (NGFC)-type cortical and hippocampal interneurons, have distinct molecular, anatomical and physiological properties. However, the molecular mechanisms regulating their diversity remain poorly understood. Here, via single-cell transcriptomics, we show that the obligate NMDA-type glutamate receptor (NMDAR) subunit gene *Grin1* mediates subtype-specific transcriptional regulation of gene expression in MGE-derived interneurons, leading to altered subtype identities. Notably, MGE-specific conditional *Grin1* loss results in a systemic downregulation of diverse transcriptional, synaptogenic and membrane excitability regulatory programs. These widespread gene expression abnormalities mirror aberrations that are typically associated with neurodevelopmental disorders, particularly schizophrenia. Our study hence provides a road map for the systematic examination of NMDAR signaling in interneuron subtypes, revealing potential MGE-specific genetic targets that could instruct future therapies of psychiatric disorders.

Keywords: Interneurons, Medial ganglionic eminence, PV, SST, Neurogliaform, NMDA receptor, Transcriptional regulation, Neurodevelopmental disorders, Schizophrenia, NMDA-hypofunction, Hippocampus, Frontal Cortex, Mouse model, scRNAseq

Email addresses:

vivek.mahadevan@nih.gov (Vivek Mahadevan),

ryan.dale@nih.gov (Ryan Dale),

tim.petros@nih.gov (Timothy J. Petros),

mcbaic@mail.nih.gov (Chris J. McBain) *Corresponding author.

17 Introduction

18 Medial ganglionic eminence (MGE)-derived forebrain GABAergic interneurons com-
19 prise the parvalbumin-containing (PV) and somatostatin-containing (SST) subpopulations
20 throughout the entire forebrain accounting for approximately 60% of all cortical interneu-
21 rons [1, 2]. In addition, approximately half of all hippocampal neurogliaform-type cells
22 (NGFCs), the so called Ivy cells, originate from the MGE [3, 4]. Interestingly, though only
23 rarely found in rodent neocortex such MGE-derived NGFCs are significantly more popu-
24 lous in primate neocortex, including humans [5]. While PV neurons exert robust somatic,
25 and proximal dendritic inhibition, the SST and NGFCs mediate domain-specific dendritic
26 inhibition on their downstream pyramidal neuron targets [6]. Collectively these classes of
27 interneurons shape diverse aspects of cortical and hippocampal circuit maturation during
28 development, and critically regulate information processing in mature circuits by maintain-
29 ing appropriate excitation-inhibition (E-I) balance [7]. Recent evidence indicates a critical
30 role for activity, particularly through ionotropic glutamate receptors (iGluRs), in driving
31 the morpho-physiological maturation of MGE-derived interneurons [8–12]. Unlike mature
32 interneurons where iGluRs differentially contribute towards synaptic transmission, imma-
33 ture and migrating interneurons express different glutamate receptor subunits including the
34 NMDA-type iGluR (NMDAR) and AMPA/Kainate-type iGluR (AMPA/KAR) [13–15]
35 prior to the expression of any functional synapses. This becomes particularly important
36 as the developing brain contains higher ambient glutamate levels than the adult brain [16].
37 Collectively, higher ambient glutamate, developmental expression of iGluRs and recruitment
38 of glutamatergic signaling is considered to be trophic [8, 17, 18] and thought to engage mech-
39 anisms to regulate various aspects of interneuron development including morphological and
40 electrical maturation to promote appropriate circuit integration [9, 11, 14, 16, 19–22].

41 Interneuron-specific impairments are increasingly considered central to the etiology of
42 multiple neurodevelopmental and circuit disorders [23]. The importance of interneuron-
43 expressed iGluRs is most notable in psychiatric disorders exhibiting impaired NMDAR-
44 associated systems [24, 25]. In the adult brain, acute pharmacological NMDAR blockade re-
45 sults in circuit disinhibition and psychotic symptoms [26], mediated in-part, by the enhanced
46 sensitivity of interneuronal NMDARs to their antagonists [27]. Indeed, direct blockade of in-
47 terneuron activity also precipitates distinct behavioral deficits relevant to schizophrenia [28].
48 In particular, ablation of the obligate NMDAR subunit gene *Grin1* in interneuron-specific
49 early postnatal mouse [29], but not PV-specific [30], or glutamatergic neuron-specific *Grin1*
50 ablation [31], resembles global *Grin1*-mutants [32] in their constellation of schizophrenia-like
51 behavioral aberrations. This indicates that *Grin1* dysfunction across multiple interneuron-
52 subtypes precipitates schizophrenia-like abnormalities [33]. In addition, this interneuron-
53 specific NMDAR-hypofunction model is sensitive to developmental age, since adult-onset
54 *Grin1* loss does not result in the same phenotypes [29]. Despite the importance of develop-
55 mental NMDAR function in interneurons, and its relevance to human neurodevelopmental
56 disorders, a comprehensive interrogation of the impact of developmental NMDAR ablation
57 in interneurons, particularly across MGE-derived interneurons, is lacking.

58 It is clear that during the developmental window between embryonic day (ED) 13.5 and

59 postnatal day (PD) ~10 [34], a combination of innate genetic programs, external environ-
60 ment, and neuronal activity shapes interneuron subtype specification leading to remark-
61 able diversity [2, 21, 35, 36] The NMDAR signaling complex comprises an essential node
62 for regulating gene expression via excitation-transcription (E-T) coupling in mature cir-
63 cuits [37–39]. Moreover, different NMDAR subunits are widely expressed in the developing
64 brain [40] where they provide a critical source of Ca^{2+} -entry via trophic glutamate signaling
65 prior to synaptogenesis [15, 19, 41]. However, it is not clear whether the NMDAR-mediated
66 Ca^{2+} cascades in nascent and developing MGE-derived interneurons engage transcriptional
67 programs necessary for MGE-derived interneuron diversity. To investigate this, we con-
68 ditionally deleted *Grin1* in MGE progenitors that give rise to cortical and hippocampal
69 PV, SST, and NGFC subsets, using the *Nkx2-1*-Cre mouse line [3, 4, 42]. In this model,
70 *Nkx2-1*-driven Cre expression is reported in cycling/proliferating MGE cells, well before the
71 cells become postmitotic, allowing for assessment of the developmental impact of embry-
72 onic loss of *Grin1* activity across all subsets of MGE-derived interneurons. Applying high-
73 throughput single-cell RNA sequencing (scRNAseq), we establish that NMDAR-mediated
74 transcriptional cascades promote MGE subtype identity, by regulating the expression of di-
75 verse transcriptional, synaptogenic and membrane excitability genetic programs. Notably,
76 we identify numerous disease-relevant genes that are misexpressed in MGE-derived interneu-
77 rons upon *Grin1*-ablation, providing a broad road map for examination of MGE-subtype
78 specific regulation via NMDAR signaling.

79 Results

80 scRNAseq recapitulates cardinal MGE subtypes and a continuum of 81 molecular profiles

82 To examine the molecular heterogeneity of MGE-derived GABAergic interneurons
83 by scRNAseq, we microdissected frontal cortex (CX) and hippocampus (HPC) from
84 fresh brain slices obtained from PD18-20 *Nkx2.1*-Cre:Ai14 mouse (**Figure1A, Figure1-**
85 **Supplement1A**). Ai14-TdTomato (TdT⁺) single-cell suspensions were harvested by
86 fluorescence-activated cell sorting (FACS) using stringent gating constraints including via-
87 bility and doublet discrimination (**Figure1-Supplement1B**) as previously described [43–
88 45], and subsequently processed through the 10X Genomics Chromium controller. 9064 and
89 9964 TdT⁺ cells were recovered from cortex and hippocampus respectively across 3 biolog-
90 ical replicates. To minimize the effect of excitotoxicity and stress-related transcriptional
91 noise, the tissue processing, FACS, and sample collection steps were performed in buffers
92 supplemented with Tetrodotoxin (TTX), DL -2-Amino-5-phosphonopentanoic acid (APV)
93 and Actinomycin-D (Act-D) [46]. Because we observed concordant cell clustering across the
94 replicates during preliminary analysis by Seurat v3 [47, 48] (**Figure1-Supplement2A**),
95 the replicates were pooled for in-depth analysis. Subsequent clustering and marker gene
96 analyses revealed that ~ 62% and 33% of the TdT⁺ MGE-sorts from cortex and hippocam-
97 pus respectively, express classical GABA markers including *Gad1 / Gad2*, *Lhx6*; and the
98 MGE-subclass markers *Pvalb*, *Sst*, and *Lamp5*, marking PV and SST, NGFC subsets respec-
99 tively (**Figure1B, Figure1-Supplement3A**). While we did not recover cells expressing

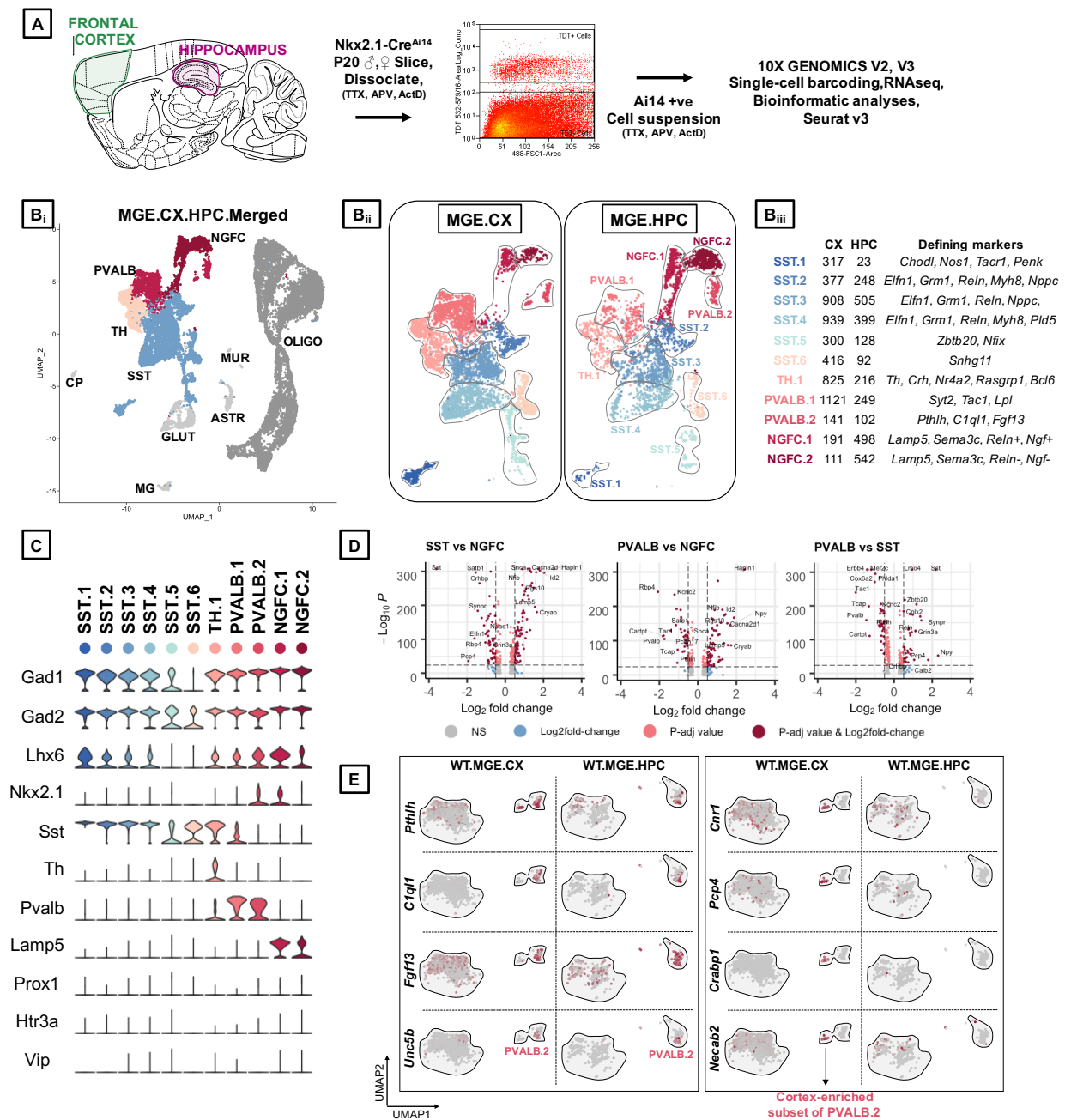


Figure 1: Identification of MGE-derived interneuron subtypes in the cortex and hippocampus.

A, Overview of the experimental workflow. **B_i**, Uniform Manifold Approximation and Projection (UMAP) dimensional reduction of 19,028 single-cell transcriptomes (9,064 from frontal cortex and 9,964 from hippocampus of 6 mouse brains), showing the cardinal MGE populations. Cell clusters were color coded and annotated *post hoc* based on their transcriptional profile identities (Cell type abbreviations: PVALB, Parvalbumin; NGFC, Neurogliaform; TH, Tyrosine Hydroxylase; SST, Somatostatin; GLUT, Glutamatergic; CP, Choroid Plexus; MG, Microglia; ASTR, Astrocyte; MUR, Mural; OLIGO, Oligodendrocyte). **B_{ii}**, UMAP visualization of 11 MGE-derived interneuron subtypes from cortex (MGE.CX) and hippocampus (MGE.HPC), and the recovery of cell numbers from the subtypes. **B_{iii}**, Table indicating the number of *Gad1/Gad2*⁺ cells recovered in each MGE subtype from the cortex and hippocampus, and the defining genes enriched in each subtype. **C**, Violin plot showing the distribution of expression levels of well-known representative cell-type-enriched marker genes across the 11 MGE subtypes. **D**, $-\log_{10}$ False Discovery Rate (FDR) versus \log_2 fold change (FC) between each of the MGE cardinal class, representing the top enriched markers at a fold change ≥ 0.5 and FDR $< 10e-25$. **E**, UMAP representation of PVALB clusters highlighting the cortex-specific enrichment of *Pthlh*-expressing PVALB.2 subtype that is not observed in the hippocampus.

100 the CGE-markers *Prox1*, *Htr3a* or *Vip*, we recovered a minor fraction of cells corresponding
101 to glutamatergic neurons, astrocytes and microglia. In addition, ~25% and 71% TdT⁺ MGE-
102 sorts from cortex and hippocampus respectively were enriched in oligodendrocytes marked
103 by *Olig1* expression across all replicates (**Figure1-Supplement 2B,2C**). However, we fo-
104 cused our subsequent analyses on the 5656 and 3002 *Gad1 / Gad2* positive cortical and
105 hippocampal MGE-derived interneurons.

106 Unbiased cell clustering by Seurat v3 identified six subtypes of SST, two subtypes of PV,
107 two subtypes of NGFCs, and one subtype of Tyrosine hydroxylase (TH) expressing interneu-
108 rons, expressing the markers *Sst*, *Pvalb*, *Lamp5* and *Th* respectively, across the two brain
109 regions examined (**Figure1C**). Notably, all but two subtypes (SST.5 and SST.6) expressed
110 high levels of *Lhx6*, and 2 clusters corresponding to PV.2 and NGFC.1 expressed *Nkx2.1*
111 at this developmental time. While the PV- SST- and NGFC- clusters clearly exhibited ro-
112 bust gene expression differences among each other (**Figure1D**), the TH cluster appeared
113 to express genes that correspond to both PV: SST clusters, including *Sst* and *Pvalb* expres-
114 sions (**Figure1C, Figure1-Supplement3B**). Particularly, at this developmental window
115 we could not observe robustly different gene expression variances between the cortical and
116 hippocampal counterparts, barring a few marginal, but significant differences (**Figure1-**
117 **Supplement4B**) . This gave us sufficient rationale to perform subsequent analyses using
118 the MGE-derived interneurons pooled from cortex and hippocampus.

119 Among the **SST sub clusters**, SST.1-5 uniquely expresses *Chodl*, *Igf2bp3*, *Cdh7*,
120 *Pld5* and *Nfix* respectively, while SST.6 expresses only markers that are common with
121 other SST clusters (**Figure1-Supplement3B**). With the exception of SST.6 the remain-
122 ing SST-expressing subclusters are described in previous scRNAseq assays (**Figure1-**
123 **Supplement5A**). For example, the *Chodl*-expressing SST.1 cluster co-express high *Nos1*,
124 *Tacr1*, *Penk*, and *Npy*, and it has been previously described as putative GABAergic long-
125 range projections neurons [49, 50]. Clusters SST.2/3/4 express *Elfn1*, *Reln* and *Grm1*
126 characteristic of putative cortical martinotti and their hippocampal counterpart, oriens-
127 lacunosum/moleculare (O-LM) [43, 51, 52](**Figure1-Supplement5B**). Lastly, *Zbtb20*-
128 expressing SST.5 is predicted to be septal-projecting interneurons [43]. Among the **PV sub**
129 **clusters**, while both PVALB.1&2 coexpresses several common markers including *Pvalb*,
130 *Kcnip2*, *Tcap* and *Kcnc1* there are several notable differences between the two clusters.
131 PVALB.1 appears to contain continuous, but non-overlapping populations expressing *Syt2*
132 representing putative fast-spiking basket cells or *Rbp4/Sst* containing putative bistrati-
133 fied cells [1, 43, 53](**Figure1-Supplement5D**) . PVALB.2 contains cells that uniquely
134 expresses *Pthlh*, *C1ql1*, *Fgf13* and *Unc5b* representing putative axo-axonic chandelier
135 cells [43, 49, 54]. We also observed a TH cluster, which, in addition to expressing several
136 genes common to the SST: PV clusters, expresses several unique genes including *Rasgrp1*,
137 *Bcl6*, *Myo1b* that segregated into mutually exclusive cluster space expressing *Crh* or *Nr4a2*
138 (**Figure1-Supplement3B, Figure1-Supplement5B**) . This cluster is also described pre-
139 viously as putative bistratified-like cells [43, 53] . Among the **NGFC sub clusters**, while
140 both NGFC.1&2 coexpress several common markers including *Lamp5*, *Hapl1*, *Cacna2d1*,
141 *Sema3c* and *Id2*, the NGFC.1 cluster uniquely expresses several genes like *Reln*, *Ngf*, *Egfr*,
142 *Gabra5* that are not expressed by NGFC.2. (**Figure1-Supplement3B**). While the *Reln*+

143 represents MGE-derived neurogliaforms, the *Reln*-population may represent putative ivy
144 cells [43] (**Figure1-Supplement5C**).

145 While the majority of the UMAP space aligns well between the cortical and hippocam-
146 pal MGE-derived interneurons, we observed some regional differences as well. (**Figure1-
147 Supplement3A_iA_{iii}**). (i) First, we observed an increase in the HPC-expressed NGFC.1&2
148 in comparison to their cortical counterparts, consistent with preferential localization of
149 MGE-derived NGFCs to HPC over CX in rodents [1, 3, 4]. (ii) Next, the *Pthlh*-expressing
150 PVALB.2 subcluster splits into two islands, only in the cortex and distinctly lacking from
151 the hippocampus. Only one of the PVALB.2 islands expresses *C1ql1*, while the other cortex-
152 enriched island expresses unique markers *Etv1*, *Cnr1*, *Pcp4*, *Crabp1*, *Necab2*, *Epha4*, *Crabp1*
153 and *Hapln1* (**Figure1E, Figure1-Supplement5D**). Whether this represents a novel sub-
154 class of chandelier cells remains to be determined. (iii) Lastly, we also observed a distinc-
155 tion in the hippocampal SST.3 corresponding to a subset of O-LM interneurons (**Figure1-
156 Supplement3A_{ii}**). The overall MGE cell numbers indicate that the SST cells account for
157 the majority of MGE cell population recovered in the scRNAseq assay from both brain re-
158 gions (**Figure1-Supplement3A_{ii}, A_{iii}**). The PV and TH clusters accounted for a greater
159 share of MGE-derived interneurons in the CX than in the HPC. While it is plausible these
160 relative cell proportions may be skewed by differential survivability of these subtypes during
161 tissue dissociation, sorting and single-cell barcoding, these relative percentages were similar
162 across biological replicates.

163 NMDAR signaling maintains MGE identities and subtype diversity

164 Because neuronal activity and glutamatergic signaling are known to regulate multiple
165 facets of interneuronal development [2, 21] [11, 36, 55], we hypothesized that the key ob-
166 ligate subunit *Grin1* and the NMDAR signaling complex may play an instructive role in
167 determining MGE subtype identities. To test whether NMDAR signaling impact the devel-
168 opment and function of MGE-derived interneurons, we ablated them in MGE progenitors by
169 crossing floxed-*Grin1* mice with the *Nkx2.1*-Cre mouse line [42]. The Earliest expressions of
170 *Nkx2.1* and *Grin1* in the developing rodent brains occur around ~embryonic day (ED) 10.5
171 and ~ED14 respectively [56–58]. Moreover, NMDAR-mediated Ca^{2+} signaling in migrating
172 interneurons are reported by ~ED16 [15]. Because the expression and activity of *Nkx2.1* pre-
173 cedes *Grin1* expression, we rationalized that utilizing *Nkx2.1*-Cre mouse will ablate *Grin1*
174 and NMDAR signaling in MGE progenitors from the earliest developmental point. We
175 sorted TdT⁺ cells from the cortex and hippocampus of *Nkx2.1*-Cre:*Grin1*^{fl/fl}:Ai14 mice and
176 performed scRNAseq using the 10X platform. The scRNAseq experiments were performed
177 using juvenile mice (PD18-20) of both sexes and from the same litters as the wildtypes (WT)
178 to enable subsequent direct comparison. Similar to the WT-datasets, the MGE-*Grin1*^{fl/fl}
179 mutants also revealed an enrichment of TdT⁺ oligodendrocytes (**Figure2-Supplement3B**),
180 however, we again focused our attention on the *Gad1/2* positive interneurons.

181 We next performed integrated analyses of the MGE-*Grin1*^{wt} and MGE-*Grin1*^{fl/fl} cortical
182 and hippocampal scRNAseq datasets. Applying similar unbiased clustering parameters used
183 for the MGE-*Grin1*^{wt} analyses, we observed a total of twelve *Gad1/2* positive clusters in the
184 integrated dataset (**Figure2A, B**). As a robust control, *Grin1* appeared to be absent or
185 vastly reduced in all MGE subsets in both brain regions from MGE-*Grin1*^{fl/fl} (**Figure2C**),

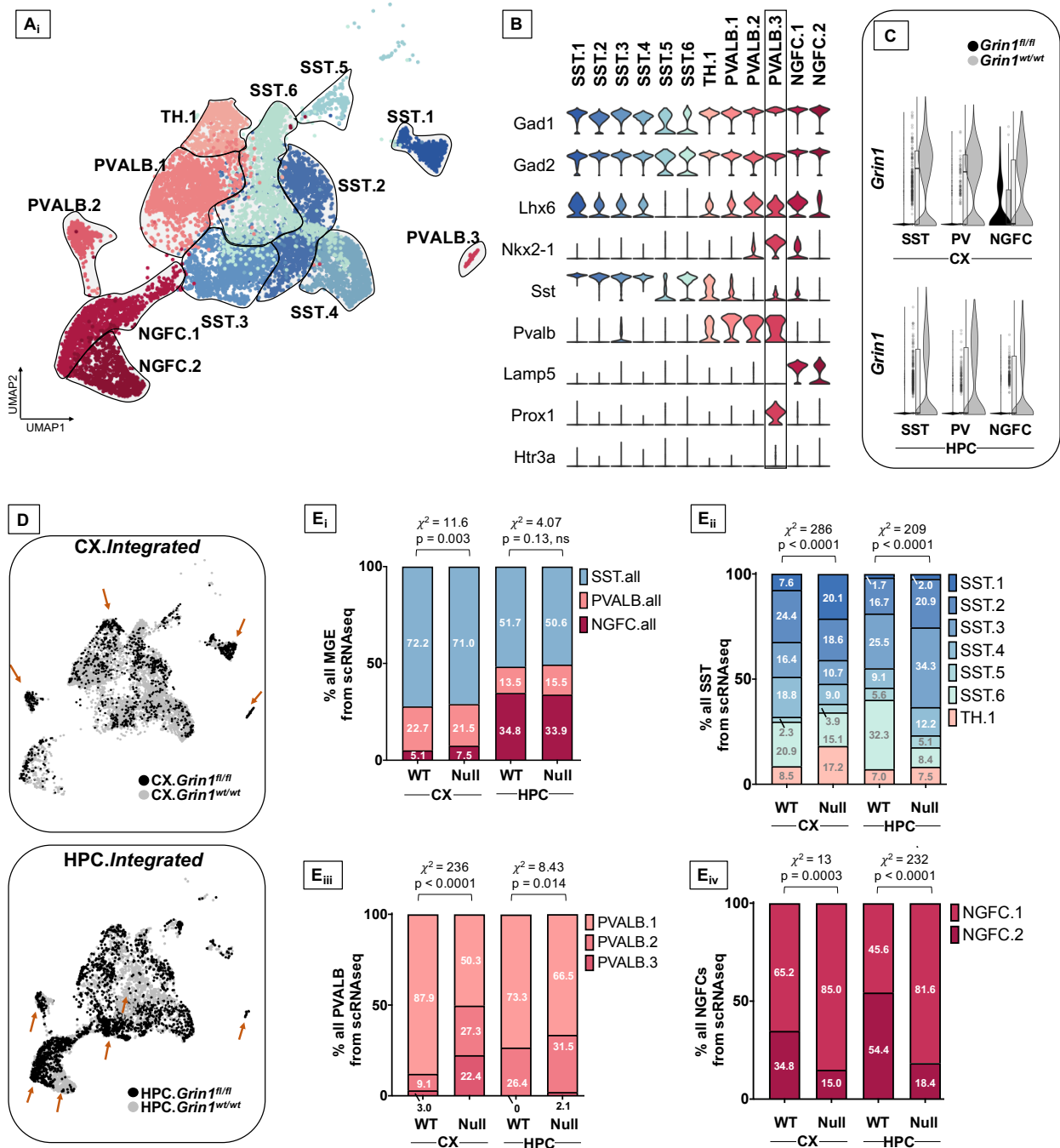


Figure 2: Altered interneuron subtype proportions upon *Grin1*-ablation

A, Integrated UMAP visualization of 12 subtypes of MGE-derived interneurons obtained from cortex (CX) and hippocampus (HPC) of *Grin1^{wt/wt}* and *Grin1^{fl/fl}* mice **B**, Violin plot showing the distribution of expression levels of well-known representative cell-type-enriched marker genes across the 12 interneuron subtypes. **C**, Violin plot from both genotypes indicating the expression of *Grin1* in the cardinal of MGE-derived interneuron subtypes. **D**, UMAP representation colored by brain-region, highlighting the differential enrichments of cells (brown arrows) within interneuron subsets in *Grin1*-WT and *Grin1*-null from CX and HPC. **E**, Stacked-barplots representing the proportions of recovered cell numbers within **E_i**, pooled cardinal MGE subtypes, **E_{ii}**, SST subtypes; **E_{iii}**, PVALB subtypes and **E_{iv}**, NGFC subtypes in *Grin1*-WT and *Grin1*-null from cortex or hippocampus. χ^2 , Chi-square test of proportions; ns, not significant.

186 but not in the *Slc17a7* expressing glutamatergic neurons (**Figure2-Supplement3A**). Over-
187 laying the WT and NULL datasets from the brain regions revealed differential enrichments
188 among the recovered cells between the genotypes (**Figure2D**). Intriguingly, *Grin1*-ablation
189 did not seem to alter the SST or PV recovery percentages, with the exception of a mod-
190 est increase in the cortical NGFCs ($\chi^2 = 11.6$, $p = 0.003$), but not hippocampal NGFCs
191 ($\chi^2 = 4.07$, $p = 0.13$) (**Figure2E_i**, **Figure2-Supplement2A_i, B**). However, we observed a
192 marked change in the recovery percentages of the subsets of SST, PV and NGFCs from both
193 cortex and hippocampus (**Figure2E_{ii-iv}**, **Supplement2A_{ii}, C**). Particularly, we observed
194 a robust increase in the *Chodl*-expressing cortical SST.1 population, and a decrease in hip-
195 pocampal SST.6 population in MGE-*Grin1^{fl/fl}*(CX, HPC: $\chi^2 = 286, 209$; p -value = $2.2e-16$
196 for both regions). In addition, we found a reduction in the cortical PVALB.1 population,
197 and a compensatory increase in PVALB.2/3 populations in MGE-*Grin1^{fl/fl}*(CX, HPC: χ^2
198 = $236, 8.4$; p -value = $2.2e-16, 0.14$). Finally, we observed an increase in the NGFC.1 along
199 with a compensatory decrease in NGFC.2 in both cortex and hippocampus (CX, HPC: χ^2
200 = $13, 232$; p -value = $0.0003, 0.14$).

201 To independently examine whether *Grin1* ablation promotes changes in interneuron
202 abundances, we conducted immunostaining experiments to probe total TdT⁺ MGE-derived
203 interneurons and the PV / SST subtypes. First, we observed no significant change in total
204 TdT⁺ hippocampal MGE-derived interneuron density between postnatal day (PD) 30-210
205 (**Figure2-Supplement1A_i**) similar to what was indicated in the scRNAseq cell recoveries
206 (**Figure2E_i**). Next, we observed a modest decrease in cortical TdT⁺ numbers at PD30,
207 which became progressively greater by PD210 (**Figure2-Supplement1B_i**), indicating dif-
208 ferent effects of *Grin1*-ablation on total MGE cell numbers in cortex and hippocampus.
209 We observed no change in hippocampal expressed total PV/SST cell type counts at PD30
210 (**Figure2-Supplement1A_{ii}**), but we noted a modest reduction in cortical PV cell type
211 counts along with an increase in cortical SST cell type counts at the same age **Figure2-**
212 **Supplement1B_i**).

213 Among the differentially enriched subclusters, *Pthlh*-expressing PVALB.3 is quite no-
214 table (**Figure2B**, **Figure2-Supplement3A,B**). This cortex-enriched cluster lacking in
215 the hippocampus was identified within the PVALB.2 putative-chandelier cells in the MGE-
216 *Grin1^{wt/wt}* (**Figure1E**, **Figure1-Supplement5D**). However, subsequent to integration of
217 the MGE-*Grin1^{fl/fl}* scRNAseq dataset, it segregated as a unique cluster, far from other
218 PVALB clusters in the UMAP space. We observed *Prox1* expression in PVALB.3, which
219 is uncharacteristic of MGE-derived interneurons, additional to robust expressions of genes
220 associated with NGFCs such as *Hapln1* and *Reln* (**Figure2-Supplement3A,B**). More-
221 over, we observed an increase in recovery of the cortical PVALB.3 cell numbers, including
222 the emergence of these cells in the hippocampus subsequent to *Grin1*-ablation (**Figure2-**
223 **Supplement2A,B**). It is unclear whether the changes in marker expression reflect a true
224 change in cell identity or whether this is reflective of alterations in relative interneuron
225 subtype proportions. Nevertheless, these data demonstrate clear changes in MGE-derived
226 interneuron subtype diversity following loss early embryonic loss of *Grin1* function.

227 **NMDAR signaling shapes the transcriptional landscape in MGE-derived**
228 **interneurons**

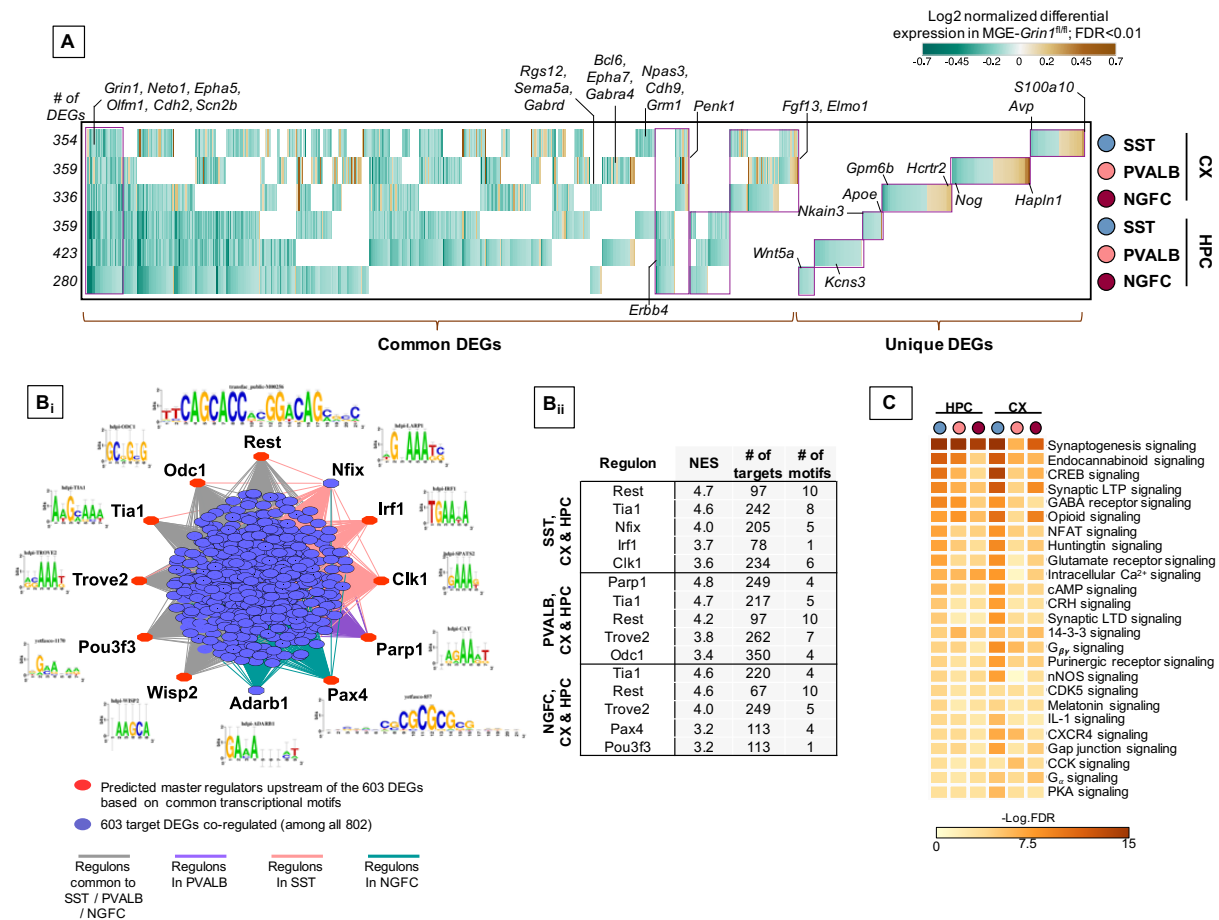


Figure 3: Cell-autonomous transcriptional changes subsequent to MGE-specific developmental *Grin1*-ablation **A**, Combined heatmap representing the 802 differentially expressed (DEGs) in the cortical and hippocampal MGE-derived interneurons upon *Grin1*-ablation, at a FDR<0.01 and FC>10%, as determined by MAST analysis (see details in Methods). **B_i**, iRegulon *in silico* analysis identifying high-confidence master upstream transcriptional regulators (indicated in red) of the DEGs (indicated in lavender). Representative DNA-binding motifs are indicated next to the transcriptional regulators. **B_{ii}**, Top five transcriptional regulators predicted by iRegulon, associated normalized enrichment score (NES) and number of predicted targets and motifs associated with each transcription factor cluster, indicated for the three interneuron subtypes (CX and HPC pooled). **C**, Ingenuity Pathway Analysis of significantly overrepresented molecular pathways in each MGE-subtype.

229 It is now well-established that transcriptional signatures defines the subtype identities
 230 of GABAergic interneurons [59]. To examine the full range of transcriptional impairments
 231 triggered by *Grin1* ablation in MGE-derived interneurons, we next performed differential
 232 gene expression testing by pooling the SST / PVALB / NGFC subtypes into their cardinal
 233 MGE classes to identify the genes that are differentially expressed between the genotypes.
 234 For instance SST1-7 and TH.1 are pooled together as SST; PVALB1-3 are pooled together
 235 as PVALB, and NGFC1-2 are pooled together as NGFC cardinal classes for this assay . At
 236 a stringent false-discovery rate (FDR) <0.01, 802 genes passed the 10%-foldchange (FC)

237 threshold across the MGE subtypes from both brain regions (**Figure3A, Supplemental**
238 **Table1**). Several interesting features were observed in the differentially expressed gene
239 (DEG) pattern upon MGE-specific *Grin1*-ablation. (i) Among all DEGs only ~10% and 1%
240 are upregulated in the cortex and hippocampus respectively, while the remaining genes were
241 all downregulated (**Figure3-Supplement1A_{ii},B,C**). (ii) While *Grin1* ablation resulted in
242 several unique DEGs between the MGE classes, ~10 and 27% of the DEGs are common
243 within cortex and hippocampus respectively (**Figure3A, Figure3-Supplement2**). For
244 instance, while *S100a10*, *Hapl1*, *Hcrt2* are uniquely upregulated in cortical SST, PV and
245 NGFC respectively (**Figure3A**), *Apoe*, *Kcns3*, *Wnt5a* were uniquely altered in hippocampal
246 SST, PV and NGFC respectively. In contrast, *Grin1* ablation induced common changes in
247 *Penk1* and *ErbB4* expression patterns across all MGE-derived interneuron classes in the
248 cortex and hippocampus respectively. (iii) ~27-43% of all DEGs were shared by MGE
249 classes across brain regions (**Figure3-Supplement2A_{ii}**). For example, *Npas3*, *Cdh9*,
250 *Grm1* are commonly downregulated in all SST subclasses; *Bcl6*, *Epha7*, *Gabra4* common
251 to PV class; and *Rgs12*, *Gabra4*, *Sema5a* common to NGFCs from both brain regions. (iv)
252 Lastly, 28 genes are commonly differentially expressed across both brain regions, across all
253 MGE subtypes. For example, *Grin1*, *Neto1*, *Cdh2*, *Scn2b* are commonly downregulated
254 across the board, while *Epha5*, *Olfm1* are commonly downregulated across all, but cortical
255 PV cells (**Figure3A**).

256 Gene expression co-regulation is intrinsic to cellular diversity [60, 61]. Since the ma-
257 jority of DEGs are downregulated across the MGE subtypes, we examined whether they
258 correspond to clusters of coordinated co-regulation. We applied the iRegulon *in silico* frame-
259 work [62], which identifies transcription factor binding motifs that are enriched in genomic
260 regions of the DEGs upon *Grin1*-ablation, and predicts the transcription factors that bind
261 to the motifs. This *in silico* analysis predicted 51 significantly enriched motifs (normalized
262 enrichment score > 3) that clustered into 10 groups by similarity, 33 of which were asso-
263 ciated with transcription factors (**Figure3B, Supplemental Table2**). Put together, 10
264 transcription factors were predicted to bind with the motifs with high confidence, strongly
265 supporting targeted co-regulation of 617 among the 802 DEG genes upon *Grin1*-ablation.
266 Notably, the RE1-silencing transcription factor (*Rest*) is a master transcriptional repressor
267 that mediates the transcriptional accessibility for several synaptic genes [63], including NM-
268 DAR subunits themselves [64]. It is intriguing to observe that the downregulation of the
269 DEGs upon MGE-specific *Grin1*-ablation are, in part, predicted to occur via *Rest*-mediated
270 transcriptional repression.

271 To examine the broad biological impact of the DEGs, we performed Gene Ontology
272 (GO) analyses. Broad GO analyses on all DEGs indicates that these genes serve to regu-
273 late multiple molecular functions in interneurons, including regulation of GABAergic and
274 glutamatergic synapses, additional to biological pathways related to addiction and circadian
275 entrainment (**Figure3-Supplement2B**). Further classification of DEGs based on their cel-
276 lular functions within the MGE subtypes revealed genes critical for regulation of membrane
277 excitability, gene expression, synaptic partnering and assembly, as well as major intracellu-
278 lar Ca²⁺ signaling cascades and second messengers (**Figure3C, Figure3-Supplement2C,**
279 **Supplemental Table3**).

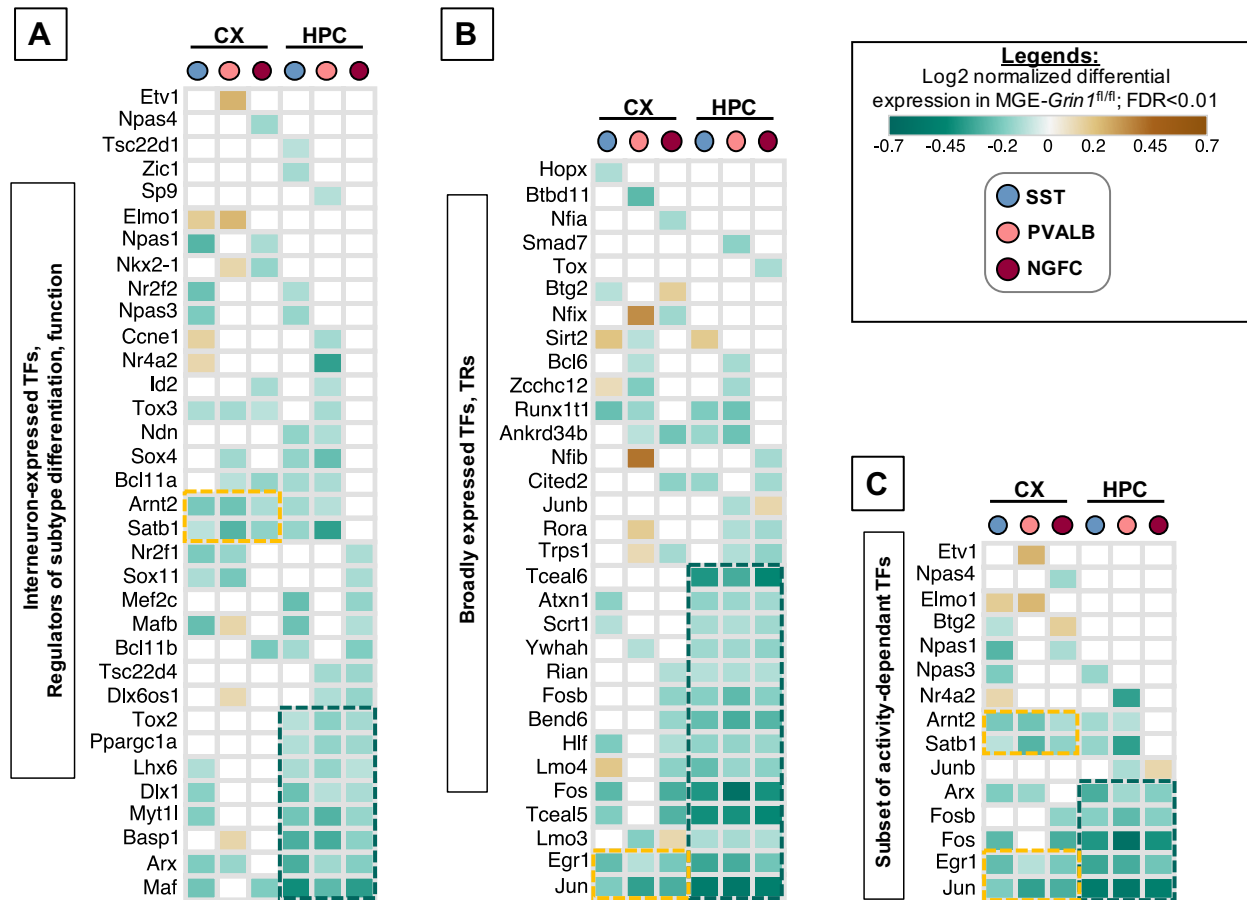


Figure 4: *Grin1*-signaling in MGE-derived interneurons are highly dedicated to the transcriptional control of interneuron identity Heatmap of log2 FC of significant DEGs in cortical and hippocampal MGE cardinal subtypes, showing a subset of **A_i**, Transcription factors (TFs) that are previously established to regulate MGE subtype identity and function; **B_i**, broadly expressed TFs and transcriptional regulators (TRs) that are not currently known to regulate MGE function; **C_i**, neuronal activity-regulated TFs. Clusters of commonly differentially expressed genes in cortex and hippocampus are indicated in yellow or green boxes.

280 Transcription factor expression is a key component of NMDAR-mediated 281 MGE regulation

282 Because transcriptional regulation underlies numerous fundamental processes including
 283 the expression of other classes of genes, we next examined the DE-transcriptional regulators
 284 in detail. We first examined the 67 genes that are differentially expressed upon *Grin1*-
 285 ablation and are known to mediate transcriptional regulation of gene expression. Of these,
 286 35 genes are previously established to be expressed in different GABAergic interneuron
 287 classes including some notable MGE-expressed transcription factors (**Figure4A_i**). The re-
 288 maining 32 are broadly expressed TFs (**Figure4B_i**), that include a small subset of 15 genes
 289 that are regulated by neuronal activity (**Figure4C_i**). Barring a few genes, we observed
 290 the majority of TFs to be down regulated in both brain regions. Intracellular Ca²⁺ sig-

291 naling cascades and second messenger systems are key mediators of NMDAR signaling to
292 the nucleus for transcriptional regulation. Theoretically, an early first wave impairment of
293 Ca^{2+} signaling in *Grin1*-lacking MGE progenitors could result in transcriptional silencing
294 of the mediators of Ca^{2+} signaling cascades and second messenger systems, which would
295 sustain the transcriptional impairments. Indeed, we also observed a downregulation of var-
296 ious Ca^{2+} homeostasis-regulators, kinases / phosphatases and second messengers that are
297 activated downstream of *Grin1* (**Figure4-Supplement1A,B,C**). Furthermore, we noted
298 that hippocampal MGE neurons had a greater proportion of DE-TFs and kinase signaling
299 cascade effectors that were downregulated across all 3 subtypes compared to their corti-
300 cal counterparts. Together, this suggests that hippocampal MGE-derived interneurons may
301 be more vulnerable than cortical MGE-derived interneurons towards *Grin1*-mediated Ca^{2+}
302 transcriptional silencing at this age.

303 Interestingly, among the early TF cascades in the progenitors that sequentially deter-
304 mine and maintain MGE fate, several members appear to be expressed at ~P20, and starkly
305 downregulated upon *Grin1*-ablation. For instance, *Lhx6*, *Maf*, *Arx*, *Myt1l*, *Dlx1* are among
306 the genes broadly downregulated across all hippocampal MGE subtypes and within spe-
307 cific class(es) in their cortical parallels (**Figure4A_{ii}**). Other MGE fate-determining TFs,
308 *Nkx2-1*, *Mafb*, *Satb1*, *Nr2f1* (CoupTf1), *Sp9*, also appear to be downregulated in discrete
309 populations. This also includes a downregulation of *Bcl11b* (Ctip2) in both hippocampal
310 and cortical NGFCs, a gene recently linked to regulation of NGFC morphology and func-
311 tion [65]. Among the few transcriptional regulators upregulated are *Sirt2*, *Elmo1*, *Zcchc12*,
312 none of which have been characterized in the context of MGE function (**Figure4B_{ii}**). *Sirt2*
313 is an established transcriptional repressor [66, 67] that may regulate the repression of sev-
314 eral target genes in an MGE-specific manner, and *Elmo1* has been previously characterized
315 during the activity-dependent migration of CGE subtypes [21]. Finally, a recent study has
316 predicted that the expression of *Zcchc12* correlates with slower intrinsic firing among hip-
317 pocampal CA1 interneurons [43]. This suggests that increased *Zcchc12* expression might
318 regulate the expression of synaptic genes enabling reduced intrinsic excitability in the MGE
319 subsets. Related to such putative decreased excitability in the MGE-derived interneurons,
320 among the activity-regulated TFs, we observe broad downregulation of *Jun*, *Egr1*, *Fos*, *Fosb*,
321 *Arc*, *Satb1*, *Arnt2* across all classes of MGE in both brain regions (**Figure4C_{ii}**). While
322 most of these are well-established activity-regulated TFs, *Arnt2* has been recently described
323 to partner with *Npas4*, downstream of Ca^{2+} signaling in response to neuronal activity [68].
324 Unsurprisingly, the *Npas*-family members *Npas1/3/4* are also downregulated in discrete
325 MGE subtypes.

326 **Impaired NMDAR signaling alters region-specific MGE subtype marker ex-** 327 **pression**

328 Several GABAergic/MGE markers were mis-regulated upon *Grin1*-ablation (**Fig-**
329 **ure5A**). For example, genes *S100a0*, *Pthlh*, *Hcrtr2* that are normally expressed in
330 SST, PV and NGFCs respectively, are upregulated in the same clusters of MGE-
331 *Grin1^{fl/fl}* (**Figure5B_i**), indicating a misexpression in a subtype-specific manner. Next,
332 while certain genes such as *Reln*, *Tenm1* are broadly downregulated across MGE classes,
333 some genes like *Thsd7a* show an upregulation in certain classes but a down regulation in

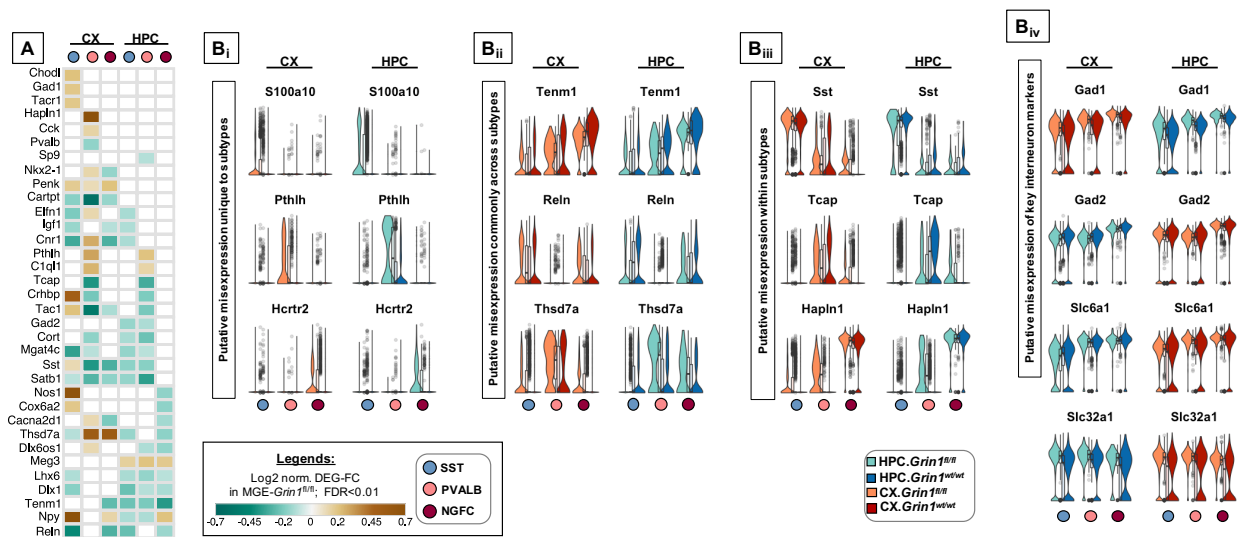


Figure 5: Fig. 5 | Differential expression of interneuron marker genes across subtypes upon *Grin1*-ablation A, Heatmap of log₂ FC of significant DEGs in cortical and hippocampal MGE cardinal subtypes, showing a subset notable MGE marker genes. Representative box-violin plots of top differentially expressed genes from the above that represent B_i, a misexpression unique to a single MGE-*Grin1*^{fl/fl} subtype; B_{ii}, a misexpression across all MGE-*Grin1*^{fl/fl} subtypes; B_{iii}, a misexpression between MGE-*Grin1*^{fl/fl} subtypes. B_{iv}, Representative box-violin plots of fundamental interneuron markers.

334 the other classes (**Figure5B_{ii}**). Interestingly, a few genes that are normally abundant in
 335 one MGE class, appear to be misexpressed in another MGE class where they are not abun-
 336 dant. For instance, *Tcap*, that is normally expressed in PV cells, in addition to being
 337 decreased in PV cells, is upregulated in NGFCs in both cortex and hippocampus. Simi-
 338 larly, *Hapln1* expression which is typically limited to NGFCs, is upregulated in PV subsets
 339 (**Figure5B_{iii}**). Lastly, we observed an upregulation in the *Gad1* and *Slc32a1* (vesicular
 340 GABA transporter, vGAT) and a downregulation in *Gad2* and *Slc6a1* (Na⁺-Cl⁻ dependent
 341 GABA transporter, GAT1), corresponding with GABA synthesis and reuptake machineries
 342 respectively (**Figure5B_{iv}**). Taken together, these data indicate that *Grin1*-ablation alters
 343 region-specific MGE subtype numbers, and subtype marker expression indicative of altered
 344 subtype identities.

345 NMDAR signaling regulates MGE subtype-specific expression of neurodevel- 346 opmental disorder risk genes

347 Interneuron-centric disease etiology is an emerging centrality in multiple psychiatric dis-
 348 orders [23]. Thus, we questioned whether the *Grin1* ablation induced DEGs presently iden-
 349 tified correlate with disease etiology. Disease-ontology based Ingenuity Pathway Analysis
 350 of the DEGs showed significant over-representation of genes implicated in ‘Schizophrenia’, ‘Psy-
 351 chiatric disorders’ and ‘Movement disorders’, among other cellular impairments involving
 352 aberrant morphology of neurons (**Figure6A, Supplemental Table4**). To independently
 353 examine the DEGs for potential enrichment for neurodevelopmental disorders, we obtained
 354 the risk genes for schizophrenia (Sz) and autism spectrum (As) from the SZDB [69] and
 355 SFARI [70] databases respectively. These databases curate and rank disease-relevant gene

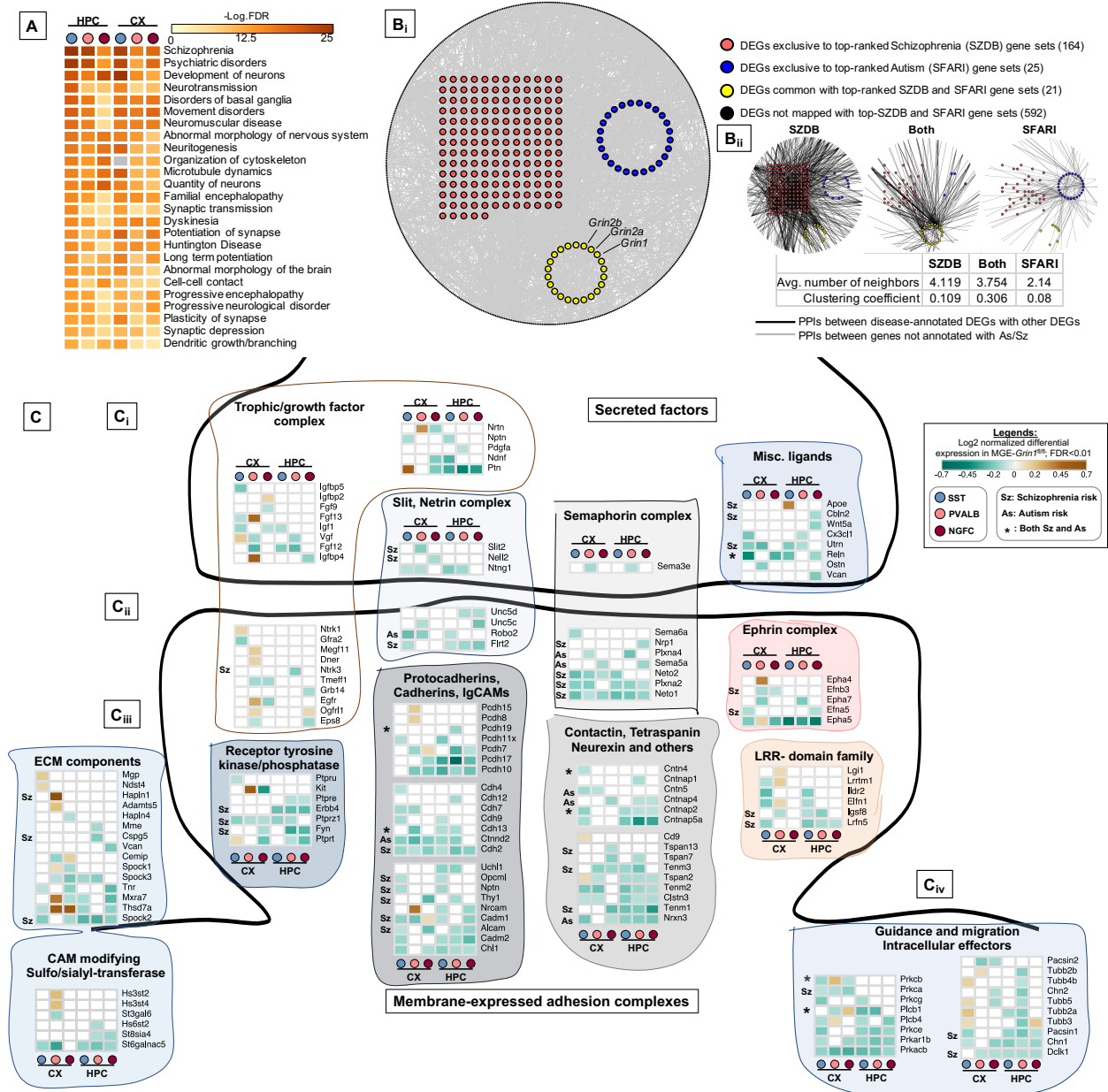


Figure 6: Aberrant *Grin1*-signaling result in misexpression of high-risk Sz genes **A**, Ingenuity Pathway Analysis of significantly overrepresented disease pathways in each MGE-subtype. **B_i**, Global protein-protein interaction (PPI)map among all differentially expressed genes (DEGs). Red circles indicate the DEGs annotated to be top-ranked Sz-risk genes; Blue circles indicate the DEGs annotated to be top-ranked As-risk genes; Yellow circles indicate the DEGs annotated with both Sz and As-risk genes. Black circles in the periphery indicate the DEGs not annotated with high-risk Sz/As genes. The PPIs between DEGs indicated in grey lines. **B_{ii}**, PPIs between Sz / As / dually enriched clusters, and other genes. The PPIs between disease-annotated DEGs and other disease-annotated DEGs or with other non-annotated DEGs are indicated in black lines. The PPI between non-annotated DEGs indicated in grey lines. **C**, Heatmap of log2 FC of significant DEGs in cortical and hippocampal MGE cardinal subtypes, showing a subset of **C_i**, secreted trophic factors and secreted ligands and guidance cues. **C_{ii}**, membrane-bound synaptogenic receptors and cell adhesion molecules (CAMs) **C_{iii}**, Extracellular Matrix (ECM) components and matrix modifying enzymes. **C_{iv}**, Intracellular effectors of guidance and synaptogenic cues.

356 sets, based on multiple evidence sources including genome-wide association studies, copy-
357 number variations, known human mutations and other integrative analyses. In particular,
358 we mapped the DEGs with the top-ranked genes from these disease datasets (see methods for
359 details). While 592 DEGs could not be mapped with either disease genes, 25 genes mapped
360 exclusively with the SFARI-AS gene list, 164 genes mapped exclusively with the SZDB-Sz
361 gene list and 21 genes mapped with both datasets (**Figure6B_i**, **Supplemental Table5**).
362 It is now well-established that several neurodevelopmental disorders exhibit a high degree of
363 converging molecular pathways employing proteins that exist in physical complexes [71–74].
364 Therefore, we examined whether these disease-associated DEGs are known to form pro-
365 tein complexes between each other, by mapping curated protein-protein interaction (PPI)
366 datasets for all 802 DEG products. Indeed, we observed that >95% of disease-annotated
367 DEG products are known to exist with PPIs, while only ~75% of DEG products not anno-
368 tated with Sz/As are known to exist with PPIs (**Supplemental Table5C**). Interestingly,
369 despite not mapping directly with the high-ranked disease gene sets, the remaining 592
370 genes are observed to exist in tightly-knit PPIs with the disease annotated genes. How-
371 ever, the PPIs mapped with SZDB form the most interconnected clusters in comparison to
372 the SFARI-mapped PPI network (**Figure6B_{ii}**), as indicated by relatively higher clustering
373 coefficient. This indicate that members of the DEGs here identified share physical, and
374 functional pathways in MGE-derived interneurons, contributing towards disease etiology.

375 Among the 210 DEGs mapped with to Sz and As, 45 genes are established regulators
376 of axon path-finding, synapse formation and assembly, while 38 members are established
377 regulators of membrane excitability and neuronal firing. Because both of these gene classes
378 are intimately associated with interneuron function, we examined these classes in detail. We
379 observed multiple classes of secreted ligands and cognate receptor families corresponding
380 to semaphorin, netrin, slit, chemokine and growth factors, and their intracellular effectors
381 that are downregulated upon MGE-*Grin1*-ablation (**Figure6C_{i,iv}**). These include *Ntn1*,
382 *Sema3e*, *Slit2*, *Cx3cl1*, and some of their receptors, *Unc5c*, *Nrp1*, *Neto1/2*, *Robo2* that are
383 decreased in a MGE-class-specific manner. We observed *Fgf13* that was recently demon-
384 strated to mediate MGE-subtype specific synapse assembly [75], to be upregulated in cortical
385 PV cells, but downregulated in cortical SST, while *ApoE* to be upregulated in hippocam-
386 pal SST cells. In addition to synaptic assembly molecules, we observed DE in a variety
387 of synaptic adhesion molecules, corresponding to protocadherin, cadherin, ephrin and con-
388 tactin families (**Figure6C_{ii}**). Notably, we also observed a downregulation of *ErbB4* across
389 all hippocampal MGE-subtypes. Lastly, we observed increased expression of extracellular
390 matrix components *Mgp*, *Ndst4*, *Hapln1*, *Adamts5*, *Mxra7*, *Thsd7a* and the matrix modify-
391 ing enzymes *Hs3st2/4* in cortical SST/PV subtypes (**Figure6C_{iii}**).

392 Among the regulators of neuronal excitability, we observed a downregulation of multiple
393 members of postsynaptic glutamate receptor subunits, GABA receptors and their associ-
394 ated partners (**Figure6-Supplement1B_{ii}**). Interestingly, while we noted a broad down-
395 regulation of several members of potassium and sodium channel subunits, a few discrete
396 members of the *Kcn*-families were upregulated in cortical PV and NGFC subtypes. Finally,
397 we also observed multiple members of presynaptic GABA synthesis, release and uptake
398 machineries including *Gad1*, *Syt2/10*, and *Slc6a1* differentially expressed in discrete MGE

399 subtypes (**Figure6, Supplement1B_i**). Collectively, these findings highlight the centrality
400 of MGE-expressed *Grin1*-signaling during synapse formation and connectivity, which when
401 aberrantly expressed, can lead to neurodevelopmental disorders.

402 Discussion

403 Centrality of MGE-derived interneuron-expressed NMDARs from juvenile 404 brain

405 NMDARs serve as critical activity dependent signaling hubs for myriad neuronal func-
406 tions due to their innate ability to directly link network dynamics to cellular calcium events,
407 and associated transcriptional coupling. Such NMDAR-dependent excitation-transcription
408 coupling is widely established in glutamatergic neurons [76], and in specific interneurons
409 using candidate approaches [77] within mature circuits. However, the detailed unbiased
410 evaluation of the transcriptional landscape of NMDAR signaling within interneurons in de-
411 veloping circuits undergoing refinement is lacking. Our study provides the first systematic
412 “fingerprinting” of the transcriptional coupling associated with NMDAR signaling, exclusive
413 to MGE-derived interneurons, providing a road map for examining NMDAR regulation of
414 MGE-derived interneurons in a subtype specific manner.

415 Our unbiased transcriptional profiling approach indicates that developmental NMDAR
416 signaling participates in MGE-derived interneuron specification by regulating the expres-
417 sion of transcription factors (67 genes), synaptogenic (53 genes) and connectivity fac-
418 tors/adhesion molecules (61 genes), and regulators of membrane excitability (78 genes),
419 among the 802 DEGs in interneurons (**Figure7**). We employed bioinformatic analy-
420 ses to examine whether system-wide downregulation of target genes can be attributed to
421 transcription-repression elements. Indeed, we identify a set of 10 transcriptional regulators
422 that commonly recognize the DNA-motifs present in the identified DEGs, including the
423 master-repressor *Rest*. Future studies are needed to examine the role of these putative re-
424 pressor and repression motifs that have not been previously associated with MGE-specific
425 transcription. However, based on broad transcriptional downregulation of target genes, we
426 can make several predictions that should guide future investigations.

427 Shaping interneuron identity and granularity amongst subtypes

428 Interneuron development from MGE is replete with combinatorial expressions of numer-
429 ous transcription factors, leading to diversity [78, 79]. Several transcription factors that are
430 impacted by *Grin1*-signaling are established regulators of MGE fate, subtype abundances
431 and identities (34 genes) including *Nkx2-1*, *Lhx6*, *Dlx1*, *Dlx6*, *Maf*, *Mafb*, *Mef2c*, *Etv1*,
432 *Npas1*, *Npas3* and *Sp9* [34, 56, 80–83] [84]. While the scRNAseq landscapes of interneurons
433 predict several transcriptomic features that would classify them as distinct ‘cell-types’ or
434 cell-states’ [49, 85, 86] [50] the precise mechanisms responsible for such granularity is still
435 emerging [2]. It is possible that NMDAR signaling in the developing interneuron progenitors
436 may provide a combinatorial cue that will couple with innate genetic programs to gener-
437 ate the diversity in interneuron subtypes. Indicating that the *Grin1*-lacking MGE-derived
438 interneurons have impaired subtype identities, we observe differential recoveries of the sub-
439 types within SST, PV and NGFC in the scRNAseq assay (**Figure2-Supplement2A,B,C**).

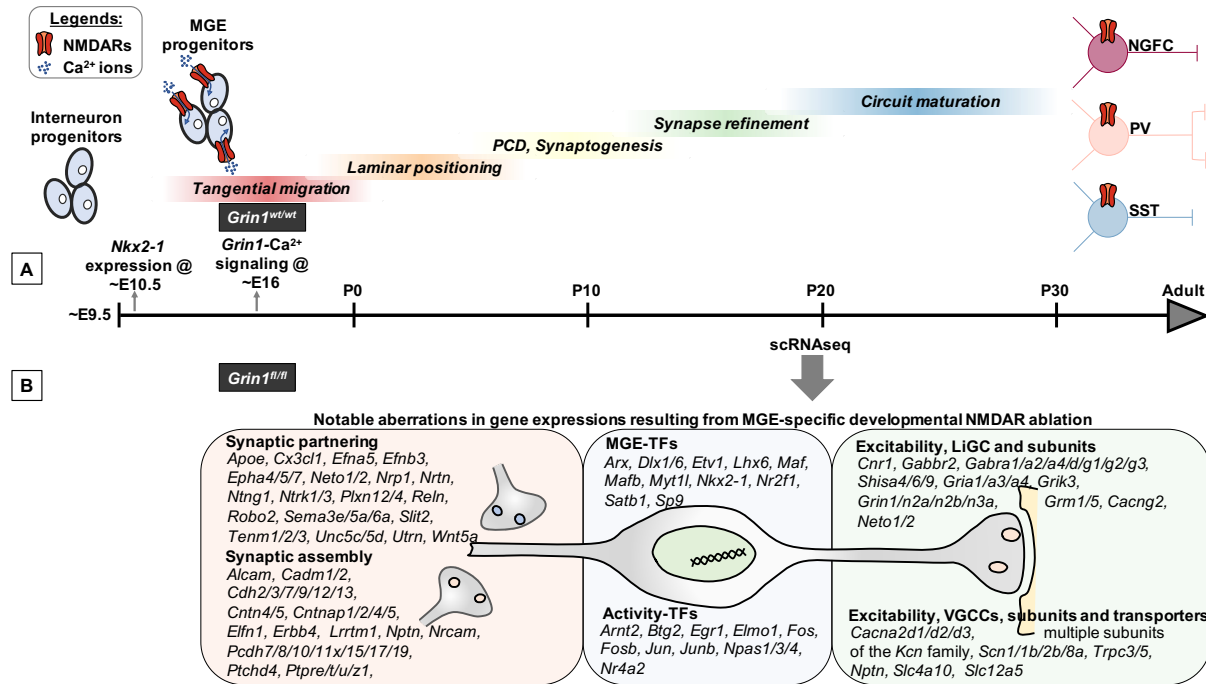


Figure 7: Transcriptional control of MGE development, synaptic partnering and excitability are mediated by NMDAR signaling **A**, *Nkx2.1* expression appears at ~ED10.5, driving MGE subtype fate in interneuronal progenitors [42] [56]. Subsequently, their sequential developmental milestones towards circuit refinement appears to be under a combination of innate genetic mechanisms and neuronal activity. While the earliest *Grin1* expression is reported at ~ED14 in developing brain [58] [57], MGE-specific *Grin1*-mediated Ca²⁺ is recorded at ~ED16 [15]. However, the broad role played by interneuron-expressed NMDAR signaling during interneuron development until now is not well delineated. **B**, By driving *Grin1*-ablation using *Nkx2.1*-driven Cre-recombinase, we report the earliest developmental loss of NMDAR signaling, across MGE-derived interneuron subtypes. In particular, by performing scRNaseq assay in MGE-derived interneurons from the cortex and hippocampus of the mouse brain, we report a broad transcriptional aberration subsequent to loss of NMDAR-signaling. Notably, this expression abnormality involves numerous transcriptional factors, synaptogenic and regulators of interneuron excitability, that collectively establish MGE subtype identities.

ED, Embryonic day; PD, Postnatal day; PCD, Programmed cell death; LiGC, Ligand-gated channel; VGCC, Voltage-gated calcium channel

440 Particularly, we find in the *Grin1*-ablated MGE-derived interneurons, the presence of divers-
 441 sified PVALB.3 populations that express marker genes such as *Prox1*, otherwise not robust
 442 in our scRNaseq screen from the MGE-*Grin1^{wt}*. Additionally, by independent immunos-
 443 taining experiments, we observe a modest increase in cortical SST cell numbers along with
 444 a modest decrease in cortical PV cells, in a manner similar to *Maf:Mafb*-mutants recently
 445 reported [82]. However, detailed future studies are necessary to uncover whether/how the
 446 NMDAR-dependent combinatorial transcriptional code works with innate mechanisms to
 447 generate the diversity within PV/SST/NGFC subclasses. It would be intriguing to examine
 448 whether these MGE-*Grin1*-null mice exhibit aberrations in the expression of these master
 449 MGE-regulators such as *Nkx2-1* and *Lhx6* earlier in development.

450 Shaping interneuron subtype-specific synaptic assembly and connectivity

451 What is the biological context of differential expression of the TFs, in the juvenile fore-
452 brain when MGE-derived interneuron fate is assumed to be already sealed, and subtype
453 identities established? It is emerging that some of these TFs are continually required for the
454 maintenance of MGE fate, post development [87]. One of the ways the TFs maintain MGE
455 subtype fate into adulthood, is by controlling the expression of genes that are essential for
456 ongoing interneuron function. Accordingly, we predict that NMDAR-dependent expression
457 of synaptogenic and synaptic partnering molecules regulate the assembly of synapses with
458 appropriate targets. Secreted semaphorin, ephrin, slit, netrin and neurotrophin-based sig-
459 naling systems have been investigated in GABAergic neurons, during axonal pathfinding,
460 and cell migration [88–95]. However, only recently have inroads been made into delineat-
461 ing their expression, and interaction with appropriate receptor systems in target synapses
462 during accurate synaptogenesis. In addition, the NMDAR-dependent expression of synap-
463 tic adhesion molecules will further promote stability of newly formed synapses. Here, the
464 mis-expression of diverse secreted cues, their receptors and adhesion molecules by MGE sub-
465 types during *Grin1*-ablation, provides unique insight into the molecular diversity employed
466 during synapse establishment. Our findings also reveal numerous candidates for examining
467 subtype specific synapse assembly, which are centrally regulated by NMDAR signaling. Of
468 particular interest are the family of protocadherins that are reported recently to be com-
469 monly downregulated in cortical interneurons generated from Sz patient-derived induced
470 pluripotent stem cells [96].

471 Subsequent to synapse formation nascent connections remain susceptible to strength
472 modifications according to neuronal activity. Again, NMDAR-signaling in MGE-derived in-
473 terneurons seems to regulate this process by the transcriptional regulation of the expressions
474 of both presynaptic and postsynaptic members, including excitatory and inhibitory synap-
475 tic molecules and their auxiliary subunits, as well as presynaptic GABA release machinery
476 molecules such as *Cplx1/2*, *Stx1b*, *Rab3c*. However, most dramatic is the massive down reg-
477 ulation of several members of the potassium channel subunits and their auxiliary subunits
478 across MGE subtypes, with the exception of an upregulation of a few *Kcn*-genes in cortical
479 PVs and NGFCs. While the precise impact of the diverse changes in these genes on MGE
480 firing are currently unclear, the pattern of expression of the activity-dependent transcription
481 factors provides us an indication.

482 Notable activity-dependent TFs such as *Jun*, *Egr1* are downregulated across all MGE
483 subtypes, while *Fosb*, *Fos*, *Arx* are down regulated across all hippocampal MGEs, and
484 *Satb1*, *Arnt2* are downregulated across all cortical MGEs. In addition, *Npas4*, an established
485 early-response TF [97–99] activated upon neuronal activity and Ca^{2+} influx in MGE-derived
486 interneurons [100], was downregulated in cortical NGFCs upon *Grin1*-ablation. *Etv1* was
487 previously demonstrated to be an activity-dependent TF that inversely correlates Ca^{2+} in-
488 flux, regulating the identity of a subset of PV-interneurons [80]. Remarkably, we observe an
489 increase in *Etv1* expression in cortical PV cells. Lastly, *Ostn* was recently established as an
490 activity-regulated secreted factor [101], and we observed *Ostn* to be downregulated specifi-
491 cally in cortical PV subtypes (**Figure4C_{ii}**). Together, these changes are consistent with
492 reduced neuronal activity in MGE subtypes upon *Grin1*-ablation, consistent with previous

493 reports indicating that NMDAR-antagonists can directly reduce the activity of GABAergic
494 interneurons in adult mice [27]. Interpreting the differential expressions of activity-
495 dependent genes during scRNAseq has been challenging, particularly, when these genes
496 could get activated by the very process involved in cell dissociation and sorting [102, 103].
497 However, our use of activity-blockers and actinomycin-D throughout our MGE-*Grin1*^{wt} and
498 MGE-*Grin1*^{fl/fl} scRNAseq pipelines [46], gives confidence that the differential expressions
499 of activity-dependent TFs reflect biological relevance.

500 **NMDAR signaling in NGFCs**

501 Among the MGE subtypes, the PV and SST interneurons are traditionally widely stud-
502 ied in comparison to the dendrite-targeting NGFC subtypes (that include the Ivy cells). In
503 the present study we provide the first detailed molecular insight into the cortical and hip-
504 pocampal NGFCs, subsequent to NMDAR ablation. We anticipated that these cell types
505 could be particularly susceptible to loss of NMDARs, since we previously reported that
506 NGFCs exhibit the most robust synaptic NMDAR conductances among the MGE sub-
507 types [12]. Intriguingly, while the cortical NGFCs had comparable numbers of both total
508 and unique DEGs with respect to other cortical MGE-derived interneurons (**Figure 3B**), we
509 observed far fewer total and NGFC-specific DEGs in the hippocampus, compared to other
510 hippocampal MGEs. However, based on the scRNAseq cell type recoveries, we predict an
511 elaboration of NGFC.1, and a reduction in the NGFC.2 subtype upon *Grin1*-ablation. Fi-
512 nally, NGFCs exhibited dendritic arborization impairments subsequent to impaired NMDAR
513 signaling [9, 11]. Indeed, we observe 49 genes among the DEGs (**Supplemental Table 1**
514) that have established roles in regulating neuronal cytoskeleton and associated signaling,
515 likely mediating the observed dendritic impairments in NGFCs.

516 **Developmental NMDAR ablation in interneurons and schizophrenia**

517 Impaired NMDAR function observed during human NMDAR gene mutations [104], and
518 anti-NMDAR-encephalitis [105] results in a wide range of neuropsychiatric disorders in-
519 cluding autism spectrum disorders [106, 107], intellectual disability [108], psychosis [109],
520 epilepsy and associated comorbidities [110, 111]. While broadly aberrant NMDAR signaling
521 in neurons is thought to underlie a wide range of these neurological disorders, an interneuron-
522 centric developmental NMDAR aberration is emerging central to schizophrenia-related syn-
523 dromes. Indeed, in the present study, disease mapping of the DEGs using high-ranked
524 SZDB-Sz and SFARI-As datasets indicate that many more DEGs map with the Sz than
525 the As database. Moreover, these disease-relevant DEGs exist in physical and functional
526 complexes with other DEGs that are not directly mapped to the Sz database. We used only
527 stringent, high-ranked disease genes from the database that pass several disease-relevant cri-
528 teria. However, there are other DEGs that still map to lower-ranked Sz and As datasets that
529 are ‘non-annotated’ in present study. While our study can be argued as an ‘extreme’ case
530 of NMDAR hypofunction in MGE-derived interneurons, it provides a starting point high-
531 lighting the centrality and broad range of interneuronal NMDAR-transcriptional pathways
532 during development.

533 A multitude of studies implicate NMDAR-hypofunction specific to PV cell types as a
534 central underlying feature of schizophrenia etiology [112, 113]. However, the measurable NM-
535 DAR conductances within PV interneurons are relatively small in comparison to other MGE

536 subtypes [12]. Additionally, NMDA signaling in non-PV interneuron subtypes drives robust
537 dendritic inhibition in pyramidal neurons [114, 115]. Moreover, while NMDAR-ablation in
538 *Pvalb*-Cre lines produces other behavioral deficits unrelated to the Sz-like phenotypes [30, 33]
539 , a developmental, but not adult-onset *Grin1*-ablation in *Ppp1r2*-Cre line [29] that targets
540 a subset of PV interneurons among other subtypes [116], recapitulates core Sz-like pheno-
541 types. Lastly, studies that map interneuron subtypes to Sz-like phenotypes indeed support
542 the role of different interneuron classes beyond PV cells towards disease etiology [28, 33].

543 Integrating these ideas and based on findings from the present study, we propose the
544 following: (i) Despite a smaller NMDAR conductance in PV interneurons, we observe a ro-
545 bust transcriptional coupling via NMDARs, as observed by several distinct gene expression
546 abnormalities in this cell type relevant to human Sz. Therefore, PV-expressed NMDARs pri-
547 marily serve to regulate transcriptional coupling, mediating the abundances of PV-subtype
548 abundances. (ii) The developmental window for NMDAR loss of function is particularly
549 important because, its transcriptional regulation maintains the correct synaptogenic and
550 assembly cues, which when lost, lead to disease causing-impaired connectivity. Perhaps,
551 in the *Grin1^{fl/fl}: Pvalb*-Cre mouse line, the *Grin1*-ablation occurs only at a developmen-
552 tal window when synaptic connectivity is sufficiently complete, explaining why the animal
553 model does not lead to profound Sz-like impairments. (iii) The dendrite targeting SST and
554 NGFC interneurons also exhibit robust NMDAR signaling and transcriptional coupling.
555 During aberrant NMDAR-transcriptional coupling, it is therefore likely that impaired den-
556 dritic connectivity and inhibition onto pyramidal neurons also contributes towards disease
557 etiology. Therefore, our dataset provides credence to interneuronal subtype-specific granu-
558 larilty, connectivity and excitability, all playing combinatorial and mutually-supporting roles
559 during disease etiology.

560 Taken together, our study presents a rich resource, laying the road map for systematic
561 examination of NMDAR signaling in interneuron subtypes, by providing multiple molecular
562 targets for examination in both normal and impaired circuits.

563 **Materials and methods**

564 **Contact for Reagent and Resource Sharing**

565 Further information and requests for resources and reagents should be directed
566 to and reasonable requests will be fulfilled by the Lead Contact, Chris McBain
567 (mcbainc@mail.nih.gov).

568 **Animals**

569 All experiments were conducted in accordance with animal protocols approved by the Na-
570 tional Institutes of Health. The *Nkx2.1*-Cre driver line (C57BL/6J-Tg(*Nkx2-1*-Cre)2Sand/J;
571 Cat. No. 008661 | *Nkx2.1*-Cre, Floxed *Grin1* mouse line (B6.129S4-*Grin1^{tm2Stl}*/J; Cat. No.
572 005246 | fNR1) and Ai14 reporter mouse (B6.Cg-Gt (ROSA)26Sor^{tm14(CAG-tdTomato)Hze}/J;
573 Cat. No. 007914 | Ai14, Ai14D or Ai14(RCL-tdT)-D), purchased from the Jackson Labora-
574 tory, were used to generate the MGE-derived interneuron-specific *Grin1^{fl/fl}* line. Littermate
575 MGE-*Grin1^{wt/wt}* controls, and both male and female mice were used during this study. Mice
576 were housed and bred in conventional vivarium with standard laboratory chow and water in

577 standard animal cages under a 12hr circadian cycle. Genotyping of the mice were performed
578 as indicated in the appropriate Jackson Laboratory mice catalog.

579 **Single-cell dissociation and FACS**

580 P18-20 juvenile *Nkx2-1-Cre: Grin1^{wt/wt}*: TdT⁺ and *Nkx2-1-Cre: Grin1^{fl/fl}*: TdT⁺ mice
581 were used for single-cell sequencing experiments. All mice were anesthetized with isoflu-
582 rane and then decapitated. Brain dissection, slicing and FACS sorting were carried out
583 as described [43, 44], with slight modifications. NMDG-HEPES-based solution was used
584 in all steps to enable better recovery of the cells [45] during FACS sorting and single-cell
585 bar coding. Briefly, the brain sectioning solution contained NMDG-HEPES-based high-
586 Mg²⁺ cutting solution contained 93 mM NMDG, 2.5 mM KCl, 1.2 mM NaH₂PO₄, 30 mM
587 NaHCO₃, 20 mM HEPES, 25 mM glucose, 5 mM sodium ascorbate, 3 mM sodium pyruvate,
588 2mM Thiourea, 10 mM MgSO₄*7H₂O, and 0.5 mM CaCl₂*2H₂O; it was adjusted to pH 7.4
589 with 12.1N HCl, an osmolarity of 300-310 mOsm, and carbogenated (mix of 95% O₂ and
590 5% CO₂) before use. This solution was chilled and the process of sectioning were conducted
591 on a ice-chamber in the vibratome.

592 3-4, *Nkx2-1-Cre: Grin1^{wt/wt}*: TdT⁺ or *Nkx2-1-Cre: Grin1^{fl/fl}*: TdT⁺ mice were pro-
593 cessed on consecutive days for single-cell sequencing experiments. TdT negative animals
594 were processed in parallel for initially setting FACS gate for the Tomato-channel. Across
595 the replicates, 10XMGE-Grin1-WT and 6XMGE-Grin1-null animals were used for the scR-
596 Naseq. Coronal slices containing frontal cortex and hippocampus (350mM) were cut using
597 VT-1000S vibratome (Leica Microsystems) in cold NMDG-HEPES-based high-Mg²⁺ cut-
598 ting solution. Slices were recovered in the same solution at 20°C for 30 minutes during
599 when, they were visually inspected under fluorescence microscope and micro dissected, all
600 under constant carbogenation. The recovery and microdissection were conducted in the
601 NMDG-HEPES high-Mg²⁺ solution supplemented with 0.5μM tetrodotoxin (TTX), 50 μM
602 DL -2-Amino-5-phosphonopentanoic acid (APV) and 10 μM Actinomycin-D (Act-D).

603 Cell dissociation was performed using the Worthington Papain Dissociation System
604 (LK003150) according to manufacturer instructions with minor modifications. Briefly,
605 single-cell suspensions of the micro dissected frontal cortices or hippocampus were prepared
606 using sufficiently carbogenated dissociation solution (containing Papain, DNase in Earle's
607 Balanced Salt Solution, EBSS), supplemented with 1μM TTX, 100 μM APV and 20 μM
608 Act-D. After a 60 min enzymatic digestion at 37°C, followed by gentle manual trituration
609 with fire-polished Pasteur pipettes, the cell dissociates were centrifuged at 300g for 5 min-
610 utes at 20°C, and the supernatants were discarded. The enzymatic digestion was quenched
611 in the next step by the addition of ovomucoid protease inhibitor. Albumin density gradi-
612 ent was performed on the pellets, using a sufficiently carbogenated debris removal solution
613 (containing albumin-ovomucoid inhibitor, DNase in EBSS). The resulting cell pellets were
614 resuspended in 1ml FACS buffer containing 10% FBS, 10U/μl of DNase, 1μM TTX, 100
615 μM APV and 20 μM Act-D in a 50:50 mix of carbogenated EBSS: NMDG-HEPES-based
616 cutting saline (with 1mM MgSO₄*7H₂O, it is important to not use High-Mg²⁺ in the FACS
617 buffer, as it interferes with the subsequent 10X scRNAseq reaction). Cells were placed in
618 polystyrene tubes (Falcon 352235) on ice during the FACS.

619 For single cell sorting of TdT⁺ expressing cells by FACS, resuspended cell dissociates

620 were filtered through 35mm cell strainer (Falcon 352235) to remove cell clumps. The single
621 cell suspensions were then incubated with 1mg/ml DAPI (1:500, Thermo Scientific 62248)
622 and 1mM DRAQ5 (Thermo Scientific 62251) at 4°C for 5 minutes to label dead cells and live
623 cells respectively. Samples were analyzed for TdTomato expression and sorted using a MoFlo
624 Astrios EQ high speed cell sorter (Beckman Coulter). TdT-negative cells were used as a con-
625 trol to set the thresholding FACS gate for the detection and sorting of the Ai14-TdTomato-
626 expressing cells, and the same gate was then applied for all subsequent experiments. Flow
627 data analysis and setting of sorting gates on live (DAPI-negative, DRAQ5-positive) and
628 Ai14-TdTomato-expressing cells were carried out using Summit software V6.3.016900 (Beck-
629 man Coulter). Per sample/session, 20,000 – 40,000 individual cells were sorted into a FBS-
630 pre-coated, Eppendorf LoBind Microcentrifuge tubes containing carbogenated 10ml FACS
631 buffer, that served as the starting material for 10X Genomics bar-coding.

632 10X Genomics Chromium

633 The cells were inspected for viability, counted, and loaded on the 10X Genomics
634 Chromium system, aiming to recover ~5000 cells per condition. 12 PCR cycles were con-
635 ducted for cDNA amplification, and the subsequent library preparation and sequencing were
636 carried out in accordance with the manufacturer recommendation (Chromium™ Single Cell
637 3' Library & Gel Bead Kit v2 and v3, 16 reactions). Sequencing of the libraries were
638 performed on the Illumina HiSeq2500 at the NICHD, Molecular Genomics Core facility.
639 Replicate 1 of the scRNAseq were performed using 10X v2 reaction from which, the cell
640 estimates, mean reads per cell (raw), median genes per cell respectively, are as follows Cor-
641 tical WT: 1277, 149K, 4615; Cortical NULL: 181, 159K, 4826; Hippocampal WT: 2221, 92K,
642 2578; Hippocampal NULL: 404, 154K, 4903. Replicate 2 of the scRNAseq were performed
643 using 10X v3 reaction from which, the cell estimates, mean reads per cell (raw), median
644 genes per cell respectively, are as follows Cortical WT: 3851, 22.8K, 1536; Cortical NULL:
645 2898, 23.5K, 2759; Hippocampal WT: 4600, 23.6K, 850; Hippocampal NULL: 4436, 25.8K,
646 3143. Replicate 3 of the scRNAseq were performed using 10X v3 reaction from which, cell
647 estimates, mean reads per cell (raw), median genes per cell respectively, are as follows Cor-
648 tical WT: 3960, 24.8K, 2870; Hippocampal WT: 3159, 26.9K, 2956. Representative quality
649 metrics from Replicate 2 are indicated in **Figure1-Supplement1B,C ,D,E**. Demultiplexed
650 samples were aligned to the mouse reference genome (mm10). The end definitions of genes
651 were extended 4k bp downstream (or halfway to the next feature if closer), and converted
652 to mRNA counts using the Cell Ranger Version 2.1.1, provided by the manufacturer.

653 Data processing, analyses, visualization and differential expression testing

654 Processing (load, align, merge, cluster, differential expression testing) and visualiza-
655 tion of the scRNAseq datasets were performed with the R statistical programming environ-
656 ment [117] (v3.5.1) and Seurat package (v3.1.5, a development version of Seurat v3.1.5.9000
657 was used to generate violin plots in 2C and 5B) [47, 48] . Data set preprocessing, compari-
658 son of WT- and NULL-Ai14 cells, canonical correlation analyses, and differential expression
659 of genes ($p_{adj} < 0.01$) within the same cluster between WT- and NULL-Ai14 cells were
660 performed according to default Seurat parameters, unless otherwise mentioned. Quality
661 control filtering was performed by only including cells that had between 200-6000 unique
662 genes, and that had <30% of reads from mitochondrial genes. While the WT replicates

663 had no cells above 30% mitochondrial genes, only NULL replicates from both brain regions
664 exhibited 7-12% of cells above this threshold. Suggestive of inherent biological impact of
665 *Grin1*-ablation, we repeated the clustering and subsequent analyses without excluding any
666 cells. These analyses did not alter the clustering or skew the gene list. Clustering was per-
667 formed on the top 25 PCs using the function FindClusters() by applying the shared nearest
668 neighbor modularity optimization with varying clustering resolution. A cluster resolution
669 of 1.0 was determined to be biologically meaningful, that yielded all known MGE cardinal
670 classes. Initial analyses were performed on the WT datasets separately (WT.alone), and sim-
671 ilar set of analysis parameters were applied when the WT and NULL samples were merged
672 (WT.NULL.integrated) for subsequent differential expression testing. Phylogenetic tree re-
673 lating the 'average' cell from each identity class based on a distance matrix constructed in
674 gene expression space using the BuildClusterTree() function. Overall, we identified 27, and
675 33 clusters using this approach in the WT.alone, and WT.NULL.integrated assays respec-
676 tively. The WT.alone correspond to 11 MGE.GAD1/2 clusters (**Figure1&2**), while the
677 WT.NULL.integrated assay correspond to 12 clusters (**Figure5-Supplement.1**). We first
678 searched for the top differential markers for each MGE subcluster using the FindAllMarkers()
679 function. The genes thus identified for the integrated data is presented in **Supplemental**
680 **Table1b**. Determination of MGE and non-MGE identities are performed based on existing
681 interneuron literature and other scRNAseq datasets [1, 43, 50, 53, 85, 87, 118–120]. The
682 labels from Figures 1 and 2 are matched with the top gene markers identified by the Find-
683 AllMarkers() function and the similarly named clusters in Figures 1 and 2 have the same
684 identities. Lastly, for the integrated analyses and differential expression testing, we first
685 merged the identities of the subclusters SST.1-SST.6 and TH.1, and relabelled as SST sub-
686 set; PVALB.1-3 relabelled as PVALB subset; and NGFC.1-2 relabelled as the NGFC subset
687 during subsequent analysis (**Figure3**).

688 Differential gene expression testing were performed using the MAST package within the
689 FindMarkers function to identify the differentially expressed genes between two subclusters.
690 MAST utilizes a hurdle model with normalized UMI as covariate to generate the differential
691 fold changes [121], and is known to result in underestimation of the magnitude of fold
692 change (FC) [122]. Therefore, while applying a stringent false-discovery rate <0.01, we
693 determined the minimum FC based on the control gene *Grin1*, which is the target gene
694 knocked out in MGE-derived interneuron celltypes. Notably for *Grin1*, we had previously
695 demonstrated that the NGFCs which carry maximum NMDAR component among MGEs,
696 are devoid of NMDAR current at this comparable age [9]. In the present scRNAseq assay,
697 we observe a logFC for *Grin1* ranging between -0.1 to -0.35 across both brain regions and
698 all MGE subtypes. Therefore, we determined a minimum logFC in our DEGs as ± 0.1 to be
699 meaningful. Previous studies have demonstrated the MAST approach for DEG testing to
700 be powerful in determining subtle changes in highly transcribed genes, and among abundant
701 populations, additional to under representing changes among weakly transcribed genes [121,
702 122]. Volcano plots and Heat maps for the DEG were generated using EnhancedVolcano
703 package [123] and Morpheus package <https://software.broadinstitute.org/morpheus> within
704 the R framework.

705 **Pathway analyses, PPI network mapping and disease mapping**

706 Ingenuity Pathway Analyses were conducted on the differentially expressed genes to gen-
707 erate the molecular functional annotation and to identify the biological pathways and dis-
708 ease pathways overrepresented. This tool was also used to annotate genes with their known
709 cellular functional classes. Additional Gene Ontology mapping and KEGG analyses were
710 conducted using ShinyGO [124]. Protein-protein interaction (PPI) mapping datasets from a
711 variety of curated databases [125–127] were conducted as previously described [72] [128] us-
712 ing the Cytoscape [129] platform (v3.8.0). Schizophrenia risk genes integrated from various
713 sources including genome-wide association studies (GWAS), copy number variation (CNV),
714 association and linkage studies, post-mortem human brain gene expression, expression quan-
715 titative trait loci (eQTL) and encyclopedia of DNA elements (ENCODE), were downloaded
716 from <http://www.szdb.org/> [69]. Autism Spectrum Disorder risk genes integrated from var-
717 ious sources were downloaded from Simons Foundation <https://gene.sfari.org/> [70]. SZDB
718 genes that had a integrated total score of 3-6 (1419 genes, 22% out of 6387) were consid-
719 ered ‘high-risk’ for DEG mapping (**Supplemental Table5a**). SFARI genes scored 1-2 with
720 accounting for a high strength of evidence (392 genes, 42% out of 943), were considered
721 ‘high-risk’ for DEG mapping (**Supplemental Table5b**). Transcriptional factor motif en-
722 richment search using the iRegulon [62] was also conducted using Cytoscape using default
723 parameters.

724 **Immunostaining**

725 All solutions were freshly prepared and filtered using 0.22 μ m syringe filters for parallel
726 treatments of wildtype and MGE-Grin1-null groups. Adult mice of postnatal day (PD)
727 30/60/210 were Mice were deeply anesthetized with isoflurane and perfused transcardially
728 with 1X phosphate buffer saline (PBS) and followed by the fixative 4% paraformaldehyde.
729 The brains were post-fixed in the same fixative for overnight at 4 °C for the immunostaining
730 assays. Postfixed brains were serially dehydrated using 10%/20%/30% sucrose solutions at
731 4 °C. Coronal sections (50 μ m) were cut on a freezing microtome. Immunostaining was
732 performed on free-floating sections. Tissue sections were permeabilized and blocked in 1 \times
733 PBS + 1% bovine serum albumin + 10% normal goat serum + 0.5% Triton X-100 (Carrier
734 PB) at room temperature for 2 h, followed by incubation in primary antibodies, listed below,
735 diluted with 1 \times PBS + 1% bovine serum albumin + 1% normal goat serum + 0.1% Triton
736 X-100 overnight at 4 °C. Tissue sections were then incubated with secondary antibodies,
737 listed below, diluted in Carrier Solution (1:1000), and DAPI (1:2000) at room temperature
738 for 1–2 h and mounted on Superfrost glass slides, and coverslipped using Mowiol mounting
739 medium and 1.5 mm cover glasses.

740 **Antibodies**

741 The following primary antibodies were used: mouse anti-PV (1:1000; Sigma-Aldrich
742 Cat# P3088, RRID: AB_477329), rat anti-SST (1:1000; Millipore Cat# MAB354, RRID:
743 AB_2255365). Secondary antibodies were conjugated with Alexa Fluor dyes 488 or 633
744 (1:1000; Thermo Fisher Scientific).

745 **Image acquisition and analysis**

746 Mouse brains from 4–8 different animals were used for each condition, and section depth
747 were matched between the genotypes for parallel immunostaining. Fluorescent images were
748 captured using the 10X objective of a Nikon Widefield Fluorescence, Spinning Disk Confocal

749 microscope. For all slices with immunostained or genetically reported signal, 50 μm thin
750 sections were imaged using 10x/0.45 CFI PlanApo objective (imaging settings: Numerical
751 Aperture 0.75, bit depth 16-bit, Exposure 100ms). Confocal stacks were stitched using NIS
752 Elements (Nikon) before importing them into Imaris software (Bitplane, version 9.2). Cell
753 bodies were marked in Imaris software using the ‘Spots’ function. *Nkx2-1-Cre:TdY⁺* RFP+,
754 PV+ cell bodies were detected using the automatic function, with a signal detection radius
755 of 10 μm . The Imaris ‘Quality’ filter was set above an empirically determined threshold to
756 maximize the number of detected cells while minimizing observed false positives. SST+ cell
757 bodies were marked manually using the Imaris ‘Spots’ function. ROI 3D borders around
758 hippocampus or cortex, drawn manually using the Imaris function ‘Surfaces’. Spots were
759 then split within each ROI using the Imaris function ‘Split Spots’. Overlap of RFP+ cells
760 with other markers (PV, SST) was addressed by filtering the RFP+ Spots above an em-
761 pirically determined threshold intensity in the channel relative to the marker of interest.
762 Each image with an automatic analysis by Imaris was checked by an expert and incorrectly
763 identified cell bodies were refined if required. In **Figure 5A,B** Error bars reflect standard
764 error of mean; Two-tailed unpaired t-test was performed using Prism8.

765 Author contributions

766 VM and CJM conceived the project. VM, TJP and CJM designed the experiments, DM
767 performed FACS sorting and analysis. VM, YZ, TJP performed 10X scRNAseq. VM, AM,
768 CJR, CE, RD performed 10X scRNAseq bioinformatic analyses. VM and AP conducted
769 immunofluorescent staining, imaging and analysis. CJM supervised the study. VM and
770 CJM wrote the paper and all authors edited the manuscript.

771 Acknowledgment

772 This work was supported by *Eunice Kennedy Shriver* NICHD Intramural Award to CJM.
773 We thank Steven L. Coon, Tianwei Li and James R. Iben at the Molecular Genomics Core,
774 NICHD, for RNA sequencing and bioinformatics support. We thank Vincent Schram and
775 Lynne Holtzclaw of the NICHD Microscopy and Imaging Core for imaging support, and
776 we thank Carolina Bengtsson Gonzales for assistance with improving cell viability during
777 dissociation and FACS. We also thank Xiaoqing Yuan, Steven Hunt, Daniel Abebe for
778 assistance with animal colony maintenance.

779 References

- 780 [1] K. A. Pelkey, R. Chittajallu, M. T. Craig, L. Tricoire, J. C. Wester, C. J. McBain, Hip-
781 pocampal GABAergic Inhibitory Interneurons, *Physiological Reviews* 97 (4) (2017) 1619–1747.
782 doi:10.1152/physrev.00007.2017.
783 URL <https://dx.doi.org/10.1152/physrev.00007.2017>
- 784 [2] B. Wamsley, G. Fishell, Genetic and activity-dependent mechanisms underlying interneuron diversity,
785 *Nature Reviews Neuroscience* 18 (5) (2017) 299–309. doi:10.1038/nrn.2017.30.
786 URL <https://dx.doi.org/10.1038/nrn.2017.30>

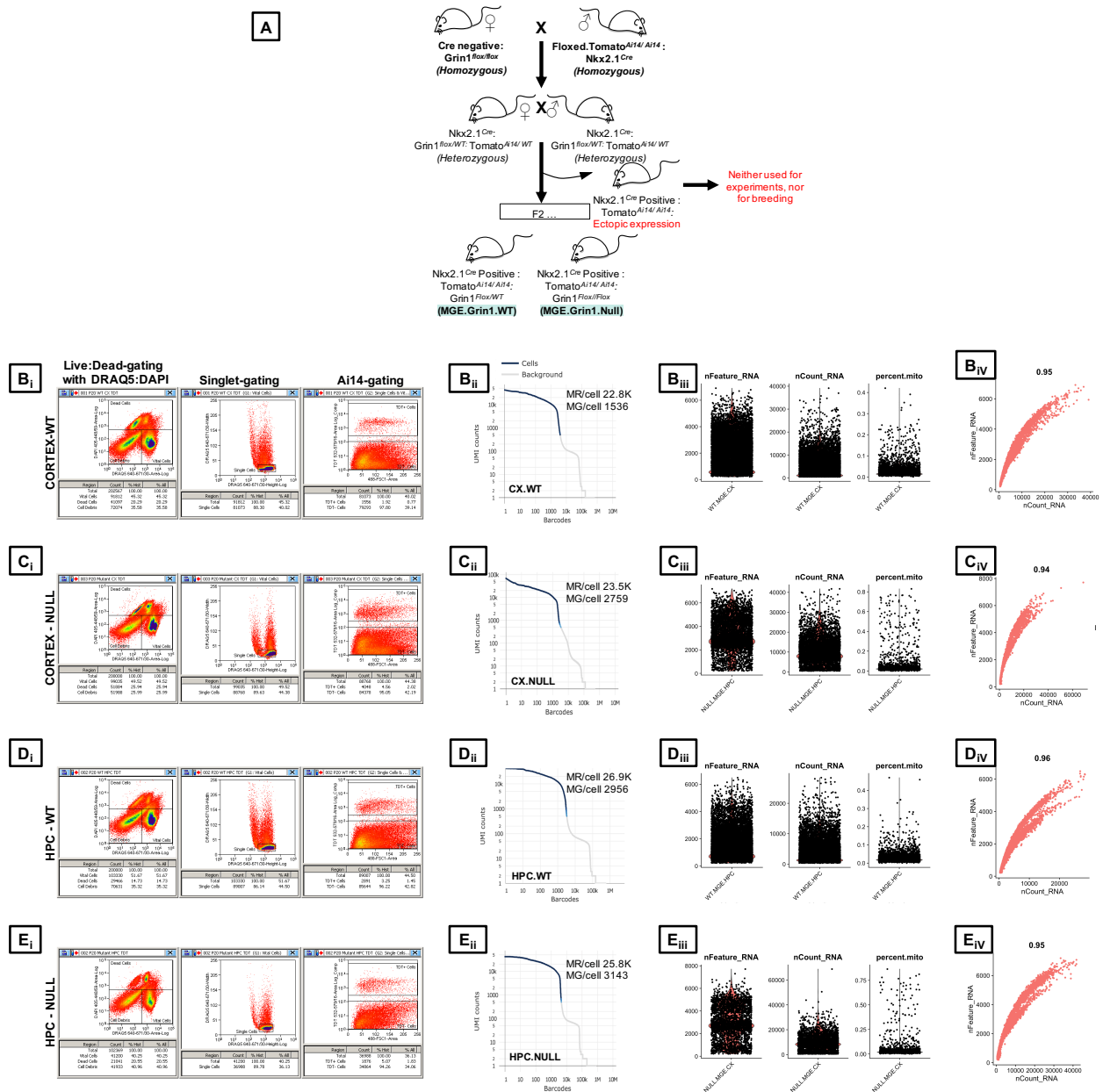


Figure 8: (Figure1, Supp.1) | Schematic overview and quality control for scRNAseq **A**, Breeding strategy, **B_i**, **C_i**, **D_i**, **E_i**, Representative FACS gates to sequentially isolate live: dead cells using DAPI: DRAQ5 staining, singlet-gating and TdT⁺-reporter gating to obtain reporter-positive MGE-derived interneurons from frontal cortex and hippocampus. **B_{ii}**, **C_{ii}**, **D_{ii}**, **E_{ii}**, Barcode Rank Plots for cells from WT and NULL mice, demonstrating separation of cell-associated barcodes and those associated with empty partitions. UMI, unique molecular identifier; MR, Mean Reads; MG, Median Genes. **B_{iii}**, **C_{iii}**, **D_{iii}**, **E_{iii}**, Distributions of the total number of genes, percentage of mitochondrial genes and UMIs per cell in control mice **B_{iv}**, **C_{iv}**, **D_{iv}**, **E_{iv}**, Pearson correlation coefficient of the distributions of the total number of genes and the UMI

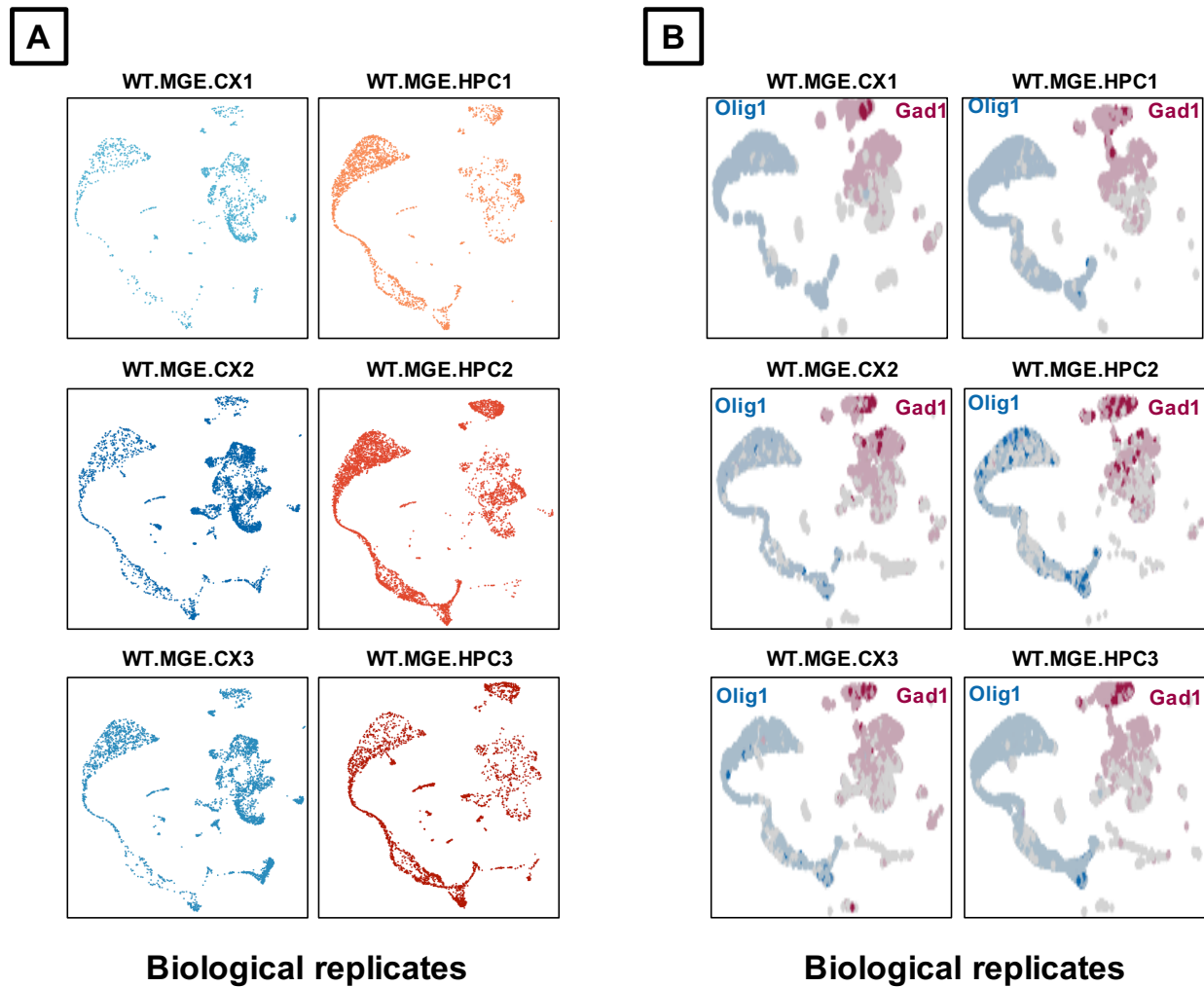


Figure 9: (Figure1, Supp.2) | **Biological replicates** Representative UMAP plots of the 3 biological replicates from cortex and hippocampus indicates **A**, similar clustering, and **B**, similar expression profiles of *Nkx2-1*-derived, *Gad1*-expressing MGE-derived interneurons and *Nkx2-1* derived, *Olig1*-expressing oligodendrocytes.

- 787 [3] L. Tricoire, K. A. Pelkey, B. E. Erkkila, B. W. Jeffries, X. Yuan, C. J. McBain, A Blueprint for the
788 Spatiotemporal Origins of Mouse Hippocampal Interneuron Diversity, *Journal of Neuroscience* 31 (30)
789 (2011) 10948–10970. doi:10.1523/jneurosci.0323-11.2011.
790 URL <https://dx.doi.org/10.1523/jneurosci.0323-11.2011>
791 [4] L. Tricoire, K. A. Pelkey, M. I. Daw, V. H. Sousa, G. Miyoshi, B. Jeffries, B. Cauli, G. Fishell, C. J.
792 McBain, Common Origins of Hippocampal Ivy and Nitric Oxide Synthase Expressing Neurogliaform
793 Cells, *Journal of Neuroscience* 30 (6) (2010) 2165–2176. doi:10.1523/jneurosci.5123-09.2010.
794 URL <https://dx.doi.org/10.1523/jneurosci.5123-09.2010>
795 [5] F. M. Krienen, M. Goldman, Q. Zhang, R. D. Rosario, M. Florio, R. Machold, A. Saunders,
796 K. Levandowski, H. Zaniewski, B. Schuman (2019).
797 [6] L. Overstreet-Wadiche, C. J. McBain, Neurogliaform cells in cortical circuits, *Nature Reviews Neuro-*
798 *science* 16 (8) (2015) 458–468. doi:10.1038/nrn3969.

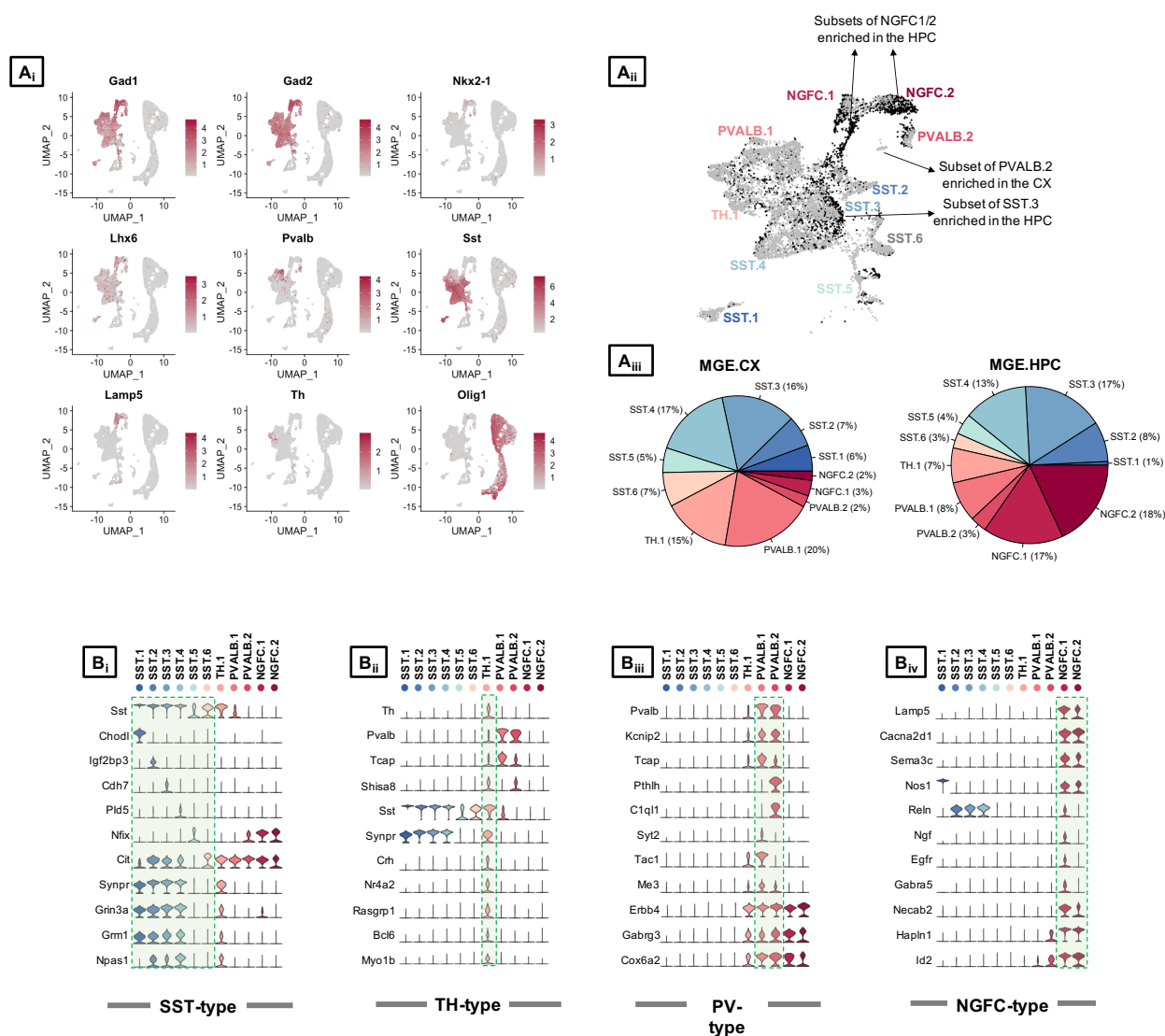


Figure 10: (Figure1, Supp.3) | Select marker gene expression across the subtypes of merged cortical and hippocampal MGE-*Grin1*^{wt/wt} **A_i**, UMAP representation of cardinal MGE markers genes in the cortical and hippocampal merged dataset. **A_{ii}**, UMAP representation colored by region, highlighting the region-specific enrichments of MGE subsets. **A_{iii}**, Pie chart indicating the percentages of cells recovered across the interneuron subtypes from cortex and the hippocampus. **B**, Violin plot showing the distribution of expression levels of well-known representative cell-type-enriched marker genes across the 11 MGE subtypes.

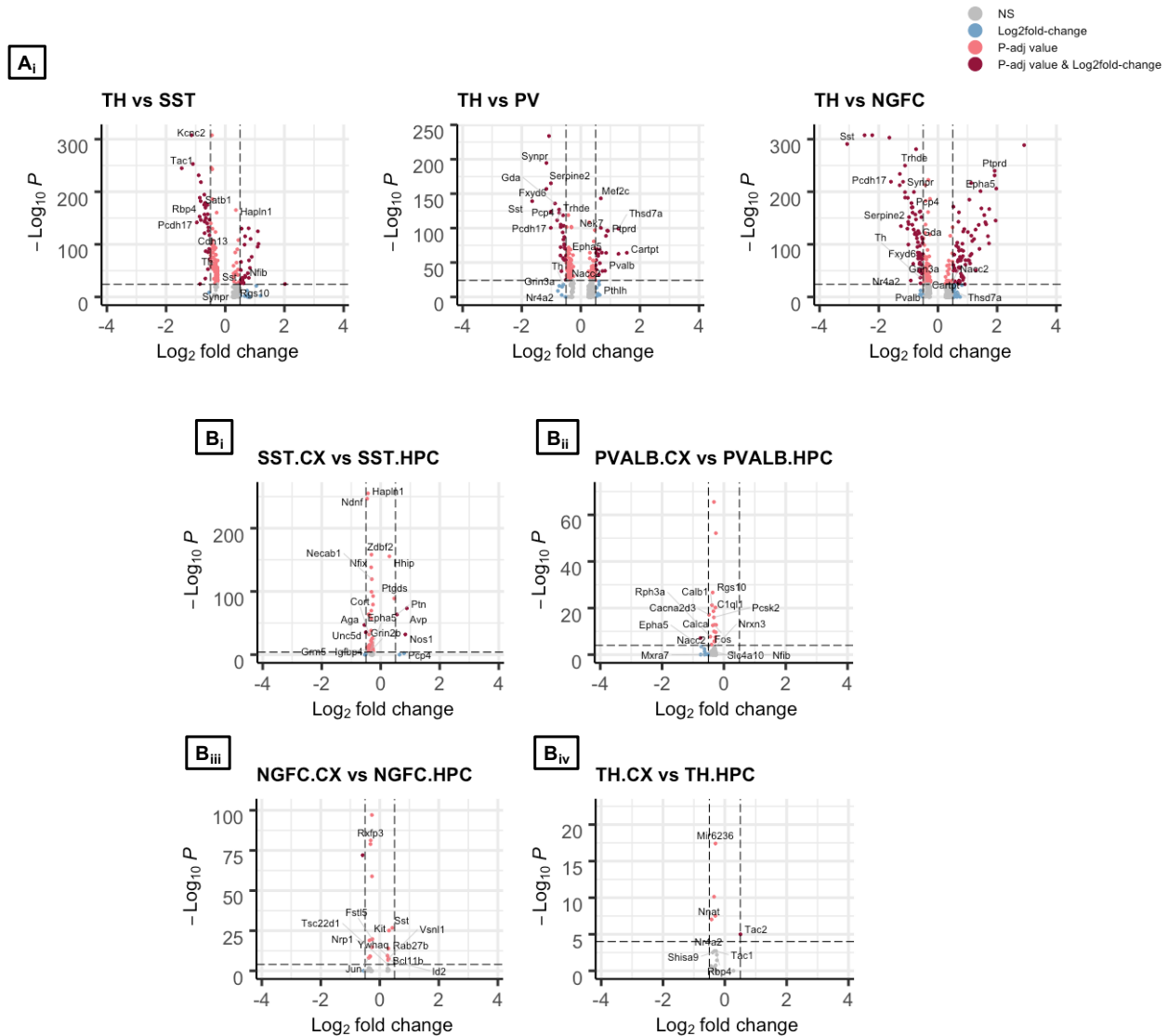


Figure 11: (Figure1, Supp.4) | MGE subtype differences between cortex and hippocampus Volcano plot representing the $-\log_{10}$ False Discovery Rate (FDR) versus \log_2 fold change (FC) between **A**, TH-expressing MGE subsets and the remaining MGE subset SST, PVALB and NGFC; **B**, Differential expression of the cardinal MGE classes between cortex and hippocampus, at a fold change ≥ 0.5 and FDR $< 10^{-5}$.

799 URL <https://dx.doi.org/10.1038/nrn3969>

800 [7] T. Klausberger, P. Somogyi (2008).

801 [8] G. Akgül, C. J. McBain, Diverse roles for ionotropic glutamate receptors on inhibitory in-
802 terneurons in developing and adult brain, The Journal of Physiology 594 (19) (2016) 5471–5490.
803 doi:10.1113/jp271764.

804 URL <https://dx.doi.org/10.1113/jp271764>

805 [9] R. Chittajallu, J. C. Wester, M. T. Craig, E. Barksdale, X. Q. Yuan, G. Akgül, C. Fang, D. Collins,
806 S. Hunt, K. A. Pelkey, C. J. McBain, Afferent specific role of NMDA receptors for the circuit integration

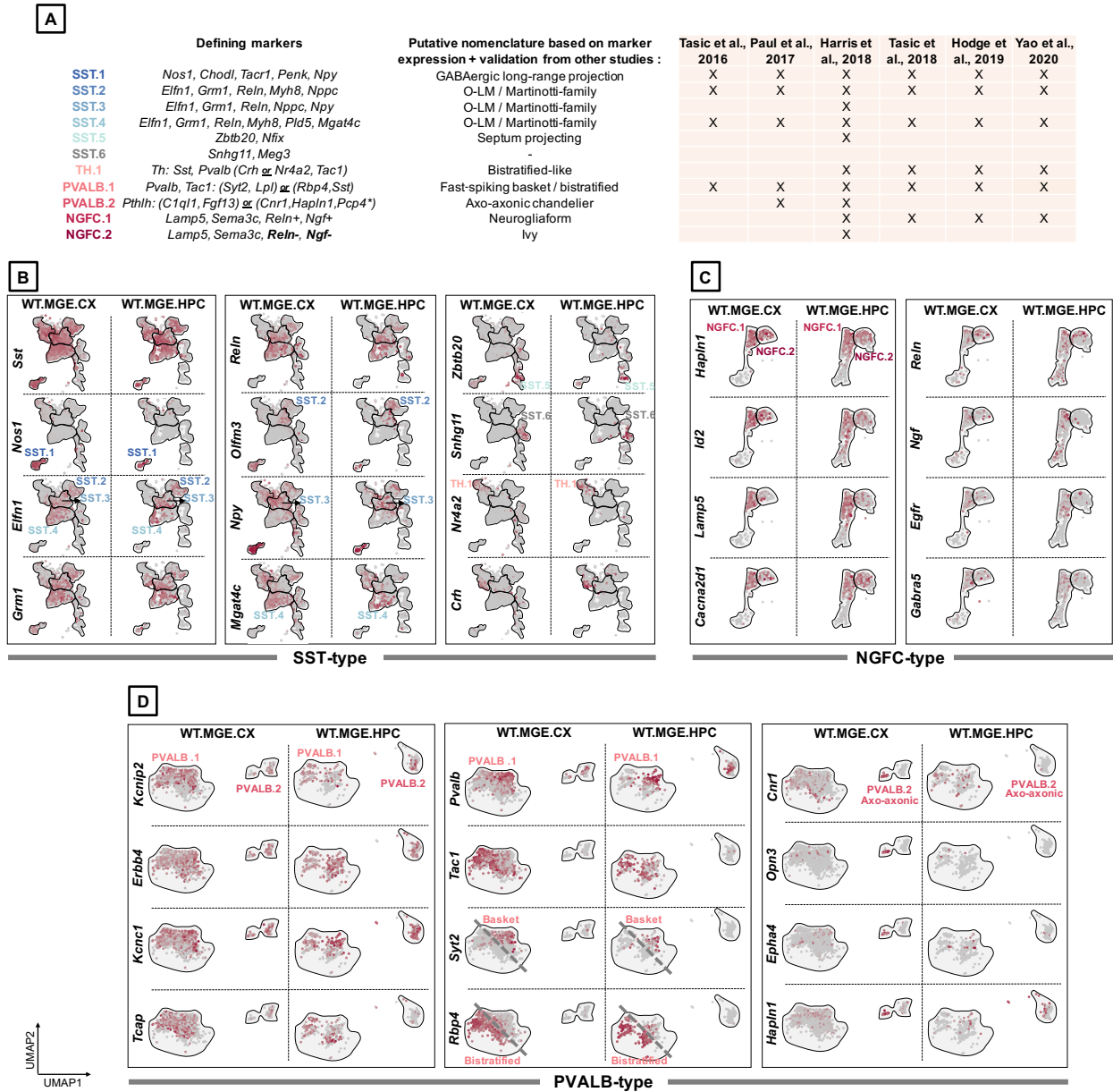


Figure 12: (Figure1, Supp.5) | MGE subtype annotation based on marker expression **A**, Table indicating the subtype-defining marker genes observed in the present study and their descriptions in the previous scRNAseq datasets (*indicates the genes expressed in the cortex-exclusive PVALB.2 subcluster). Representative UMAP plots of MGE subtype-enriched genes in **B**, SST subclusters, **C**, NGFC subclusters, and **D**, PVALB subclusters.

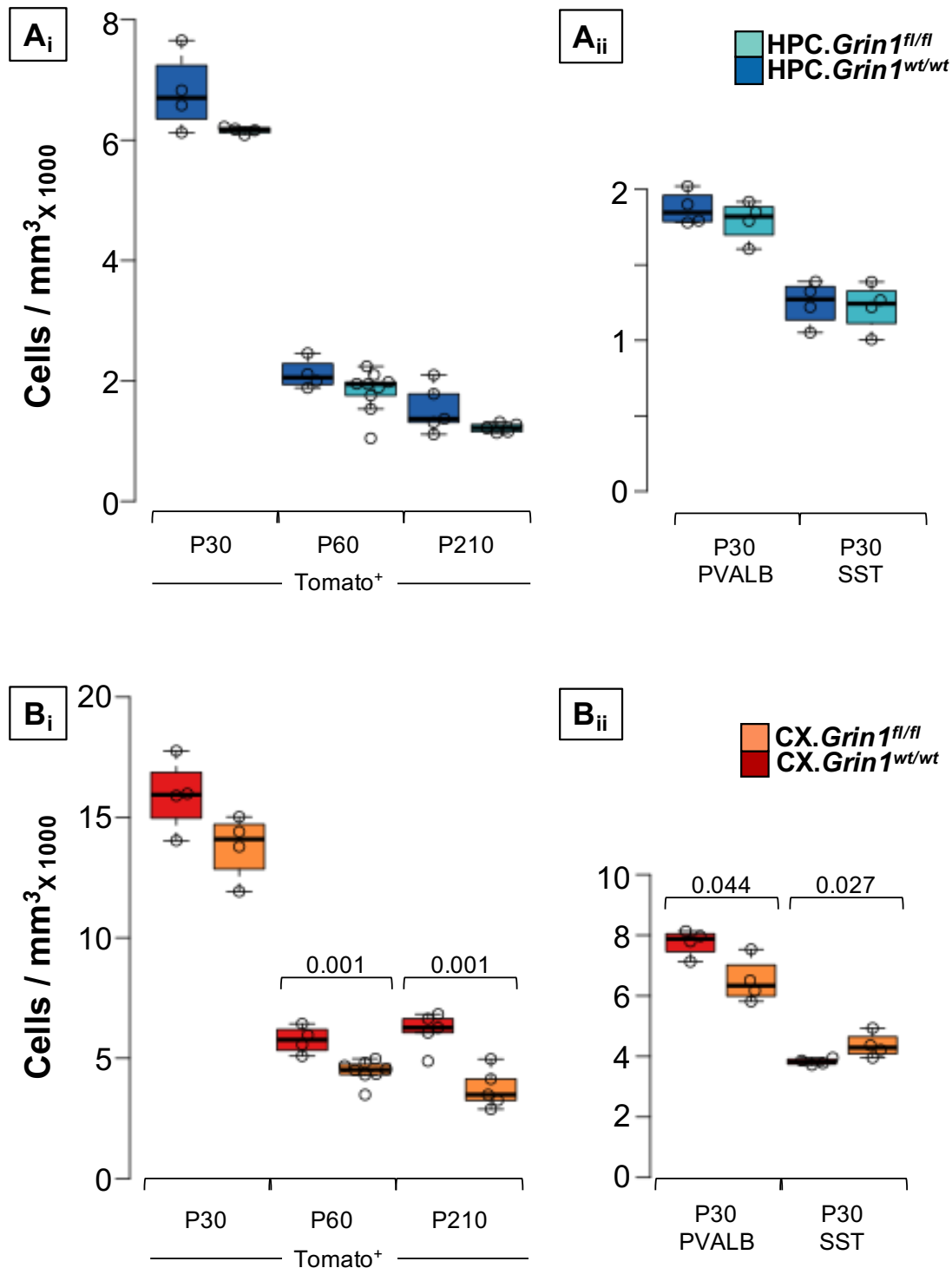


Figure 13: **Figure2, Supp.1 | MGE subtype abundances upon *Grin1*-ablation** **A**, Boxplots indicating the cell counts of hippocampal MGE-derived interneurons expressing (**A_i**) Ai14/tdTomato, (**A_{ii}**) PV, SST immunostaining from *Grin1*^{wt/wt} and *Grin1*^{fl/fl} **B**, Boxplots indicating the cell counts of cortical MGE-derived interneurons expressing (**B_i**) Ai14/tdTomato, and (**B_{ii}**) PV, SST immunostaining from *Grin1*^{wt/wt} and *Grin1*^{fl/fl}. t-test for statistical analysis.

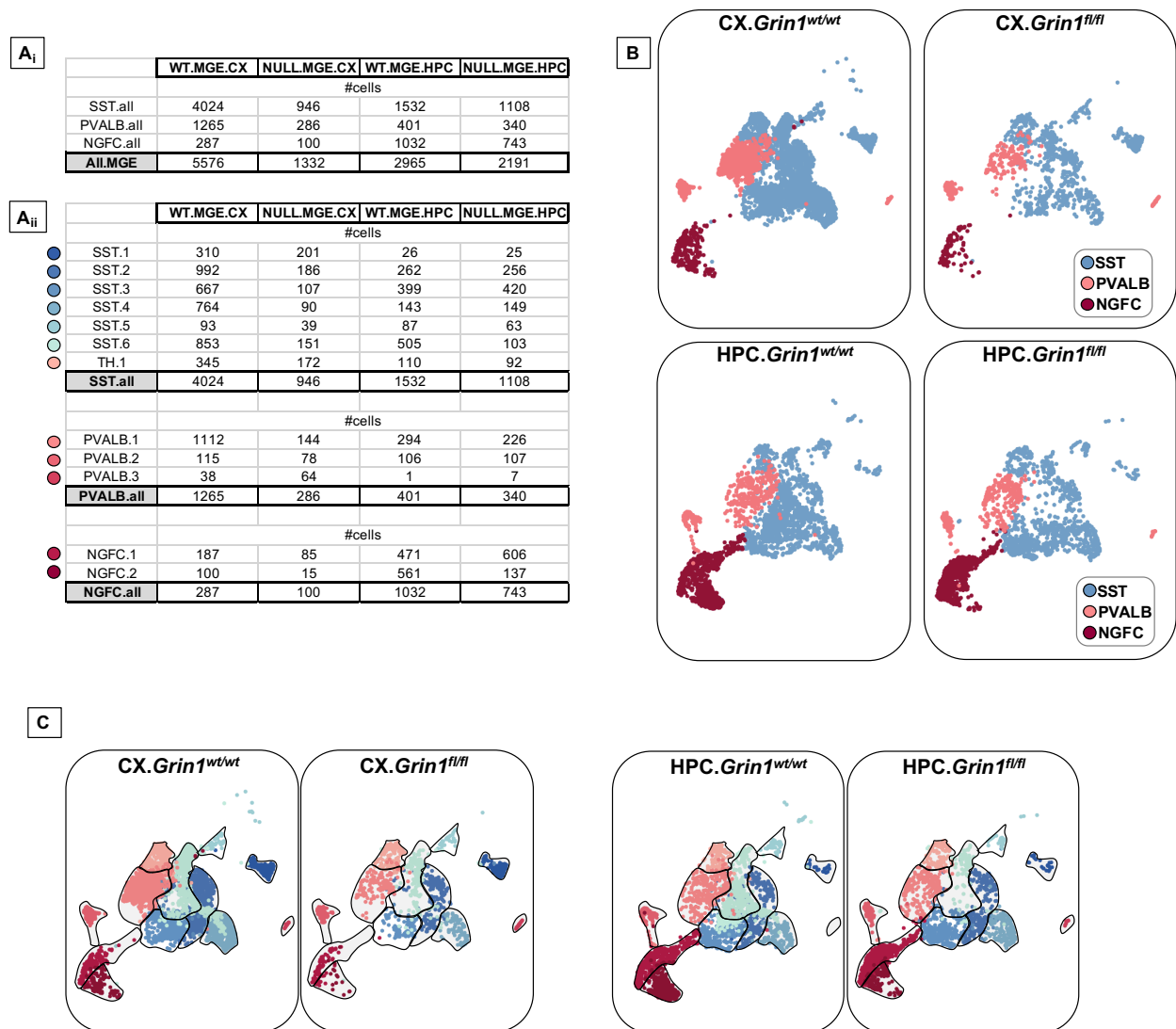


Figure 14: **Figure2, Supp.2 | scRNAseq differential recoveries of MGEsubtypes**

A_i, Number of cells recovered across cardinal subtypes SST, PV and NGFC. **A_{ii}**, Number of cells recovered within the subtypes of PV / SST/ NGFC. **B**, UMAP representation colored by cardinal MGE-derived interneuron subtypes SST, PVALB and NGFC, highlighting the differential enrichments of cells. **C**, Representative UMAP plots indicating the granularity among PV/SST/NGFC subtypes between both brain regions and both genotypes.

- 807 of hippocampal neurogliaform cells, Nature Communications 8 (1) (2017) 152–152. doi:10.1038/s41467-
 808 017-00218-y.
 809 URL <https://dx.doi.org/10.1038/s41467-017-00218-y>
 810 [10] J. H. Cornford, M. S. Mercier, M. Leite, V. Magloire, M. Häusser, D. M. Kullmann, Dendritic
 811 NMDA receptors in parvalbumin neurons enable strong and stable neuronal assemblies (2019).
 812 doi:10.7554/elife.49872.
 813 URL <https://dx.doi.org/10.7554/elife.49872>
 814 [11] N. V. D. M. García, R. Priya, S. N. Tuncdemir, G. Fishell, T. Karayannis, Sensory inputs control

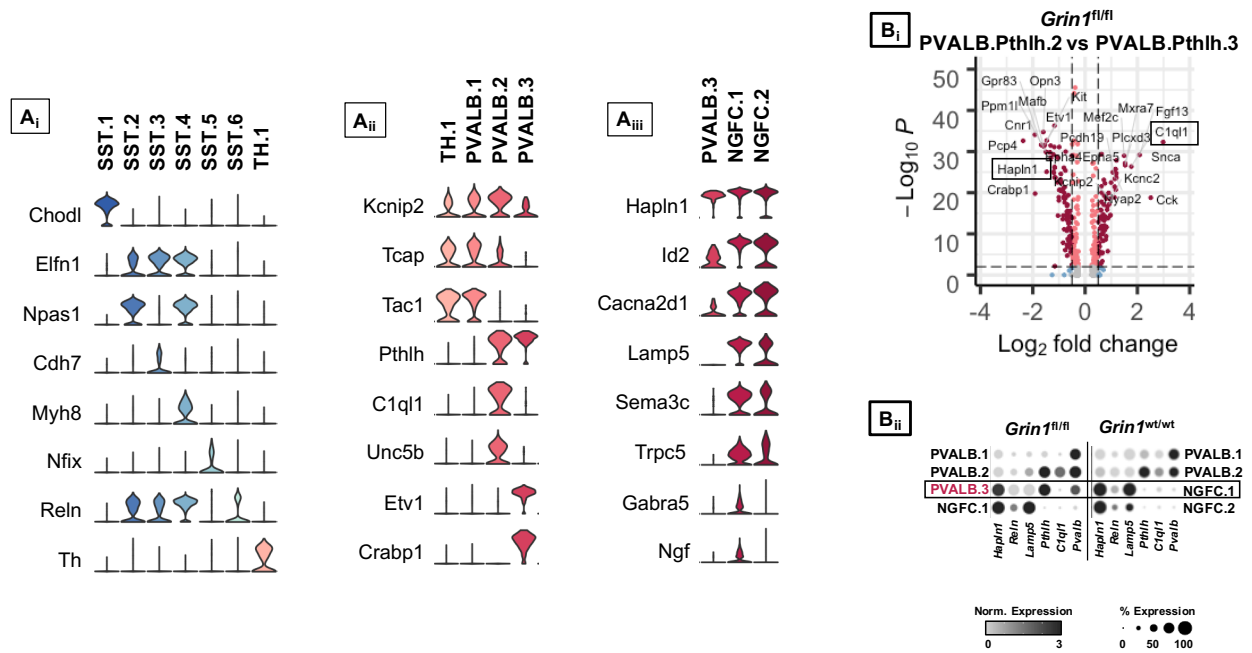
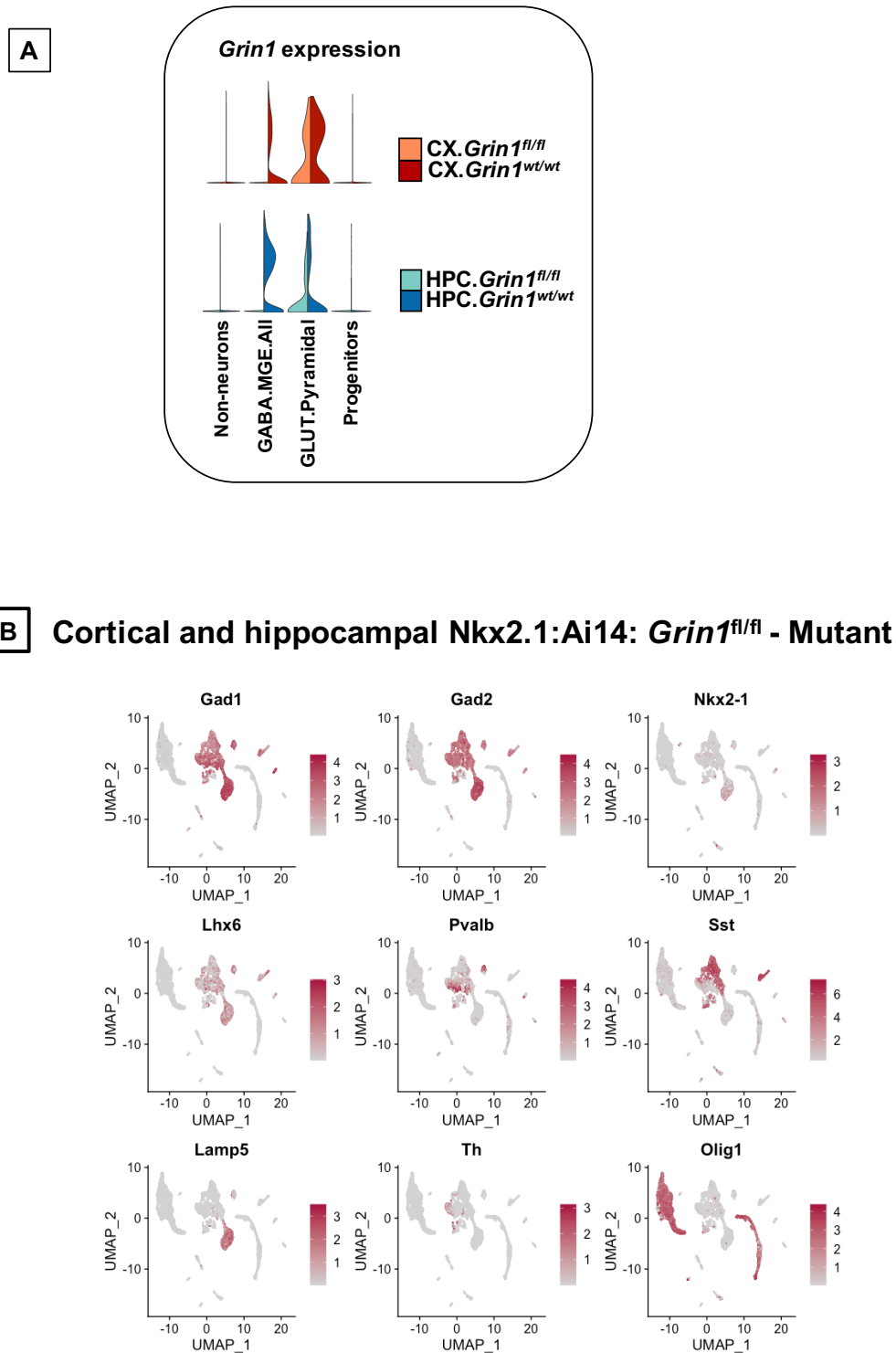


Figure 15: **Figure2, Supp.3 | Select marker gene expression across the subtypes of merged MGE-derived interneurons from *Grin1^{wt/wt}* and *Grin1^{fl/fl}*** **A**, Violin plot showing the distribution of expression levels of well-known representative cell-type-enriched marker genes across the MGE subtypes. **B_i**, $-\log_{10}$ False Discovery Rate (FDR) versus \log_2 fold change (FC) between *Pthlh*-PVALB.2 and *Pthlh*-PVALB.3 at a fold change ≥ 0.5 and FDR $< 10e-3$. **B_{ii}**, Dot plots representing the normalized expressions of NGFC marker genes mis expressed in *Pthlh*-PVALB.3 upon *Grin1*-ablation.

- 815 the integration of neurogliaform interneurons into cortical circuits, *Nature Neuroscience* 18 (3) (2015)
 816 393–401. doi:10.1038/nn.3946.
 817 URL <https://dx.doi.org/10.1038/nn.3946>
- 818 [12] J. A. Matta, K. A. Pelkey, M. T. Craig, R. Chittajallu, B. W. Jeffries, C. J. McBain, Developmental
 819 origin dictates interneuron AMPA and NMDA receptor subunit composition and plasticity, *Nature*
 820 *Neuroscience* 16 (8) (2013) 1032–1041. doi:10.1038/nn.3459.
 821 URL <https://dx.doi.org/10.1038/nn.3459>
- 822 [13] R. Luján, R. Shigemoto, G. López-Bendito, Glutamate and GABA receptor signalling in the developing
 823 brain, *Neuroscience* 130 (3) (2005) 567–580. doi:10.1016/j.neuroscience.2004.09.042.
 824 URL <https://dx.doi.org/10.1016/j.neuroscience.2004.09.042>
- 825 [14] J. B. Manent, Glutamate Acting on AMPA But Not NMDA Receptors Modulates the Migration of Hip-
 826 pocampal Interneurons, *Journal of Neuroscience* 26 (22) (2006) 5901–5909. doi:10.1523/jneurosci.1033-
 827 06.2006.
 828 URL <https://dx.doi.org/10.1523/jneurosci.1033-06.2006>
- 829 [15] J. M. Soria, Receptor-activated Calcium Signals in Tangentially Migrating Cortical Cells, *Cerebral*
 830 *Cortex* 12 (8) (2002) 831–839. doi:10.1093/cercor/12.8.831.
 831 URL <https://dx.doi.org/10.1093/cercor/12.8.831>
- 832 [16] E. Hanson, M. Armbruster, L. A. Lau, M. E. Sommer, Z.-J. Klaft, S. A. Swanger, S. F. Traynelis, S. J.
 833 Moss, F. Noubary, J. Chadchankar, C. G. Dulla, Tonic Activation of GluN2C/GluN2D-Containing
 834 NMDA Receptors by Ambient Glutamate Facilitates Cortical Interneuron Maturation, *The Journal*
 835 *of Neuroscience* 39 (19) (2019) 3611–3626. doi:10.1523/jneurosci.1392-18.2019.
 836 URL <https://dx.doi.org/10.1523/jneurosci.1392-18.2019>



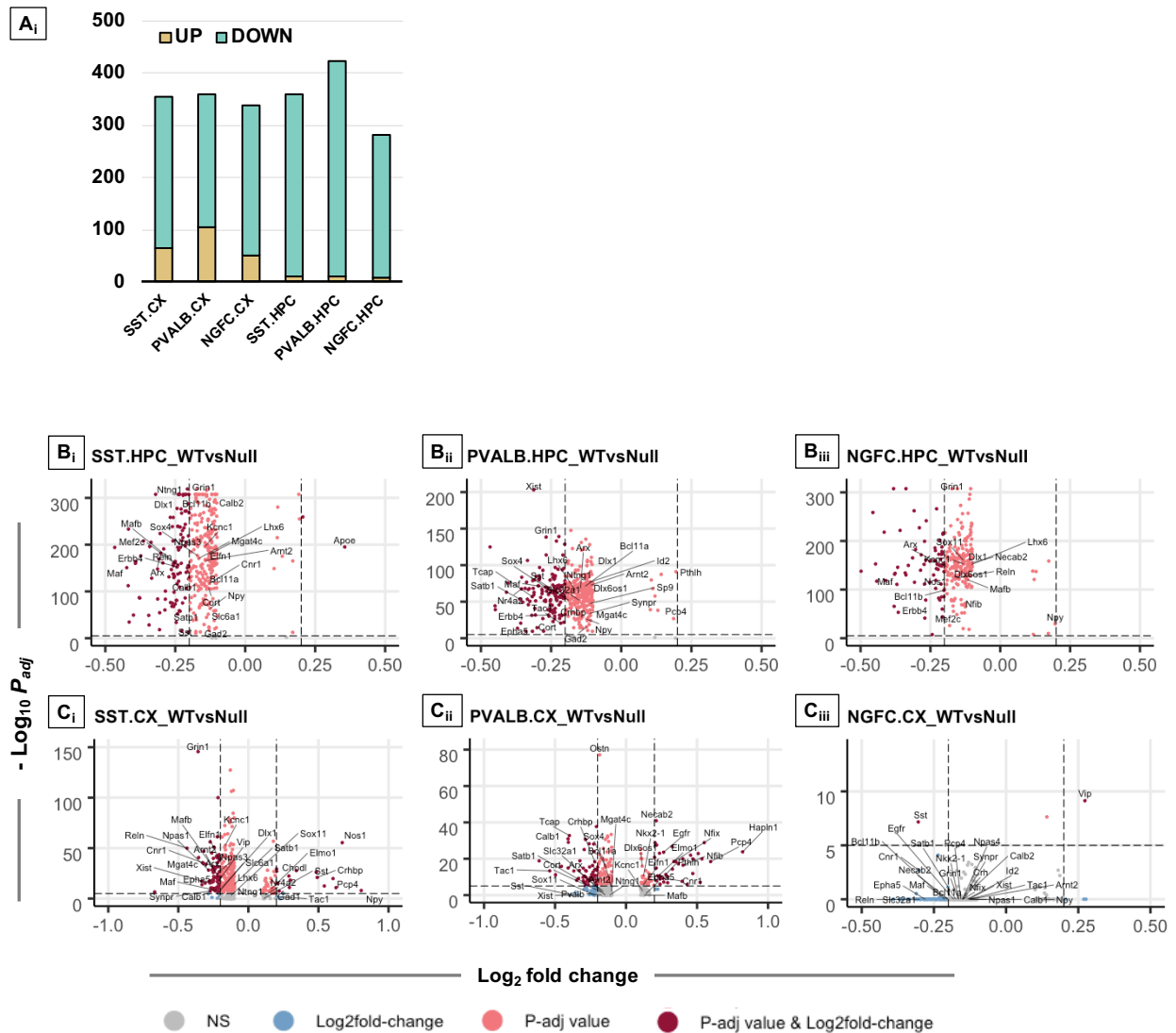


Figure 17: (Figure3, Supp.1) | Differential gene expression in the MGE subtypes subsequent to *Grin1*-ablation **A_i**, Split-violin plot from both genotypes indicating the expression of *Grin1* in the MGE-derived interneurons, pyramidal neurons and non-neurons. **A_{ii}**, Bar plot denoting the number of genes up/downregulated in the cortical and hippocampal MGE clusters. Volcano plot representing the $-\log_{10}$ False Discovery Rate (FDR) versus \log_2 fold change (FC) between **B**, hippocampal and **C**, cortical MGE cardinal clusters upon *Grin1*-loss, at a fold change ≥ 0.2 and FDR $< 10e-6$.

- 837 [17] W. Kelsch, Z. Li, S. Wieland, O. Senkov, A. Herb, C. Gongrich, H. Monyer, GluN2B-Containing
 838 NMDA Receptors Promote Glutamate Synapse Development in Hippocampal Interneurons, Journal
 839 of Neuroscience 34 (48) (2014) 16022–16030. doi:10.1523/jneurosci.1210-14.2014.
 840 URL <https://dx.doi.org/10.1523/jneurosci.1210-14.2014>
 841 [18] G. Akgül, C. J. McBain, AMPA receptor deletion in developing MGE-derived hippocampal interneurons
 842 causes a redistribution of excitatory synapses and attenuates postnatal network oscillatory activity,
 843 Scientific Reports 10 (1) (2020) 1333–1333. doi:10.1038/s41598-020-58068-6.
 844 URL <https://dx.doi.org/10.1038/s41598-020-58068-6>

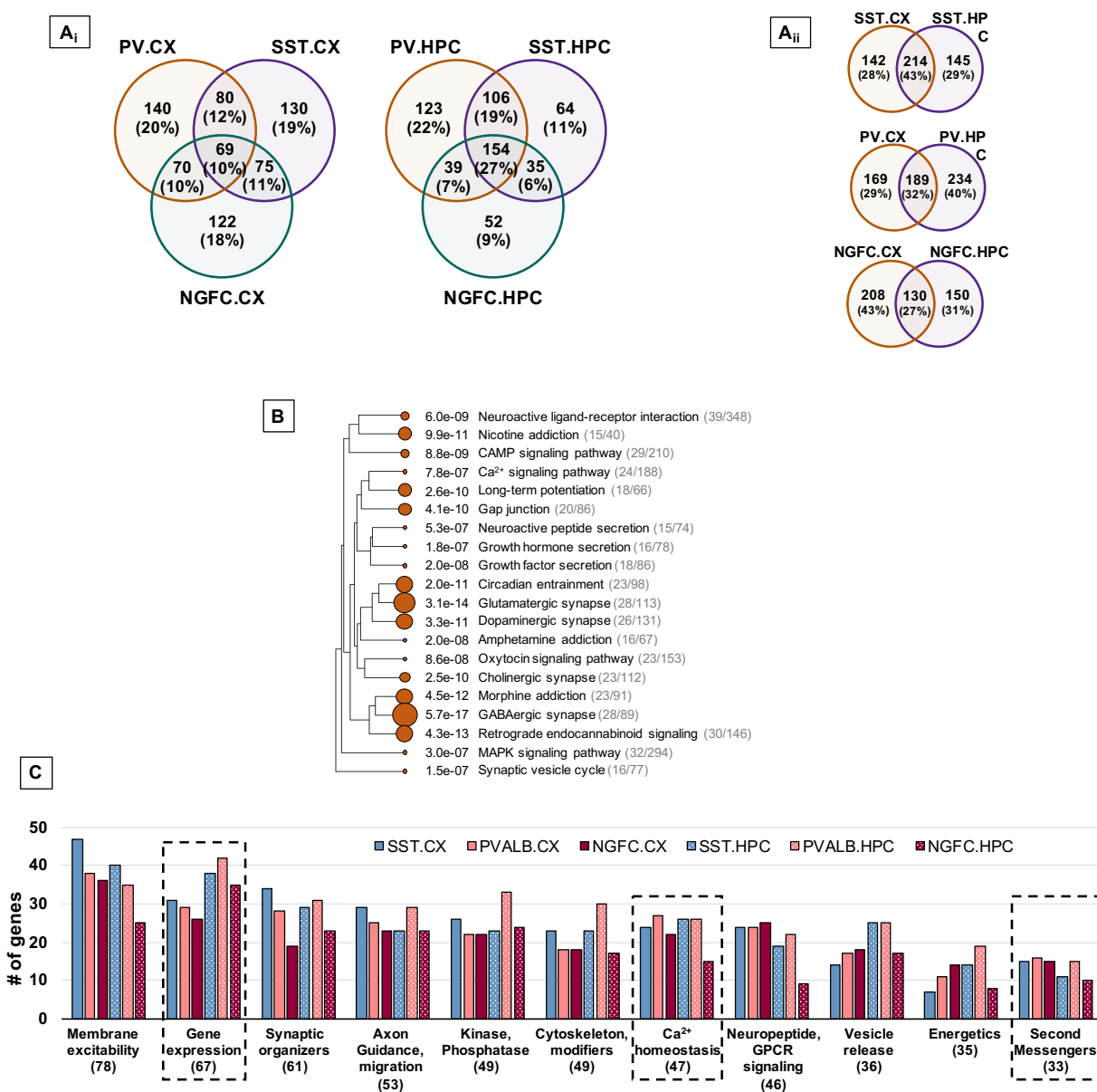


Figure 18: (Figure3, Supp.2) | Molecular pathways differentially expressed in MGE subtypes **A_i**, Venn-diagrams indicating the percentages of DEGs common within MGE subtypes from cortex or hippocampus. **A_{ii}**, Venn-diagrams indicating the percentages of DEGs common within MGE subtypes from cortex and hippocampus. **B**, Hierarchical clustering tree summarizing the correlation among significant pathways enriched among the DEGs. Pathways with many shared genes are clustered together. Bigger dots indicate more significant P-values. **C**, Bar plot showing the classification of molecular functions of the DEGs, across the MGE subtypes. Total number of DEGs in the particular molecular class indicated in parentheses.

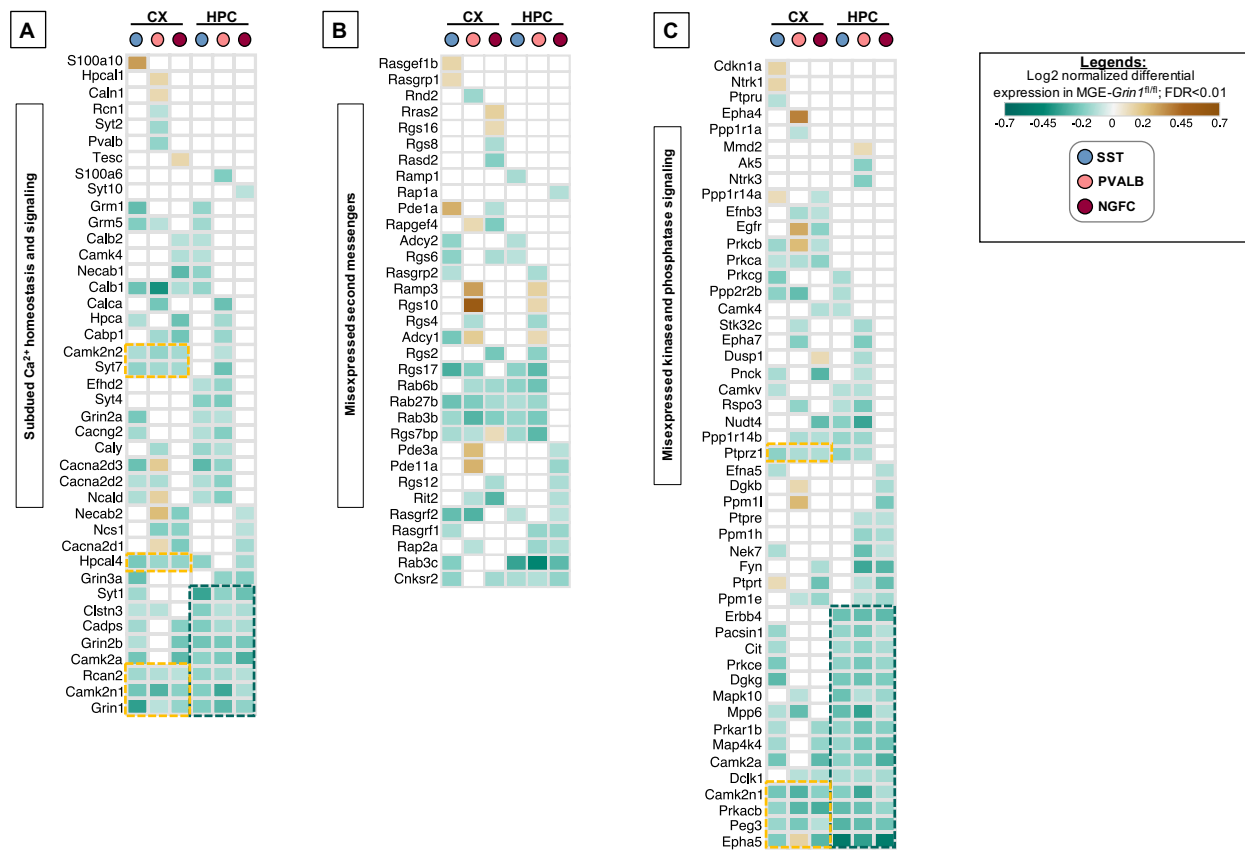


Figure 19: (Figure4, Supp.1) | Differential expression of intracellular signaling cascades across subtypes upon *Grin1*-ablation Heatmap of log₂ FC of significant DEGs in cortical and hippocampal MGE cardinal subtypes, showing a subset of **A**, genes regulating intracellular Ca²⁺ homeostasis and Ca²⁺ binding proteins; **B**, notable second messengers; and, **C**, Ca²⁺ dependent / activated kinases and phosphatases.

- 845 [19] D. Bortone, F. Polleux, KCC2 Expression Promotes the Termination of Cortical Interneu-
 846 ron Migration in a Voltage-Sensitive Calcium-Dependent Manner, *Neuron* 62 (1) (2009) 53–71.
 847 doi:10.1016/j.neuron.2009.01.034.
 848 URL <https://dx.doi.org/10.1016/j.neuron.2009.01.034>
- 849 [20] C. L. Magueresse, H. Monyer, GABAergic Interneurons Shape the Functional Maturation of the
 850 Cortex, *Neuron* 77 (3) (2013) 388–405. doi:10.1016/j.neuron.2013.01.011.
 851 URL <https://dx.doi.org/10.1016/j.neuron.2013.01.011>
- 852 [21] N. V. D. M. García, T. Karayannis, G. Fishell, Neuronal activity is required for the development of
 853 specific cortical interneuron subtypes, *Nature* 472 (7343) (2011) 351–355. doi:10.1038/nature09865.
 854 URL <https://dx.doi.org/10.1038/nature09865>
- 855 [22] M. Yozu, H. Tabata, N. König, K. Nakajima, Migratory Behavior of Presumptive Interneurons Is
 856 Affected by AMPA Receptor Activation in Slice Cultures of Embryonic Mouse Neocortex, *Develop-*
 857 *mental Neuroscience* 30 (1-3) (2008) 105–116. doi:10.1159/000109856.
 858 URL <https://dx.doi.org/10.1159/000109856>
- 859 [23] O. Marín, Interneuron dysfunction in psychiatric disorders, *Nat. Rev. Neurosci* 13 (2012) 107–120.
- 860 [24] K. Nakazawa, K. Sapkota, The origin of NMDA receptor hypofunction in schizophrenia, *Pharmacology*
 861 & *Therapeutics* 205 (2020) 107426–107426. doi:10.1016/j.pharmthera.2019.107426.

- 874 K. Takehara-Nishiuchi, J. C. Kim, Parvalbumin and GAD65 Interneuron Inhibition in the Ventral
875 Hippocampus Induces Distinct Behavioral Deficits Relevant to Schizophrenia, *Journal of Neuroscience*
876 34 (45) (2014) 14948–14960. doi:10.1523/jneurosci.2204-14.2014.
877 URL <https://dx.doi.org/10.1523/jneurosci.2204-14.2014>
- 878 [29] J. E. Belforte, V. Zsiros, E. R. Sklar, Z. Jiang, G. Yu, Y. Li, E. M. Quinlan, K. Nakazawa, Postnatal
879 NMDA receptor ablation in corticolimbic interneurons confers schizophrenia-like phenotypes, *Nature*
880 *Neuroscience* 13 (1) (2010) 76–83. doi:10.1038/nn.2447.
881 URL <https://dx.doi.org/10.1038/nn.2447>
- 882 [30] T. Korotkova, E. C. Fuchs, A. Ponomarenko, J. von Engelhardt, H. Monyer, NMDA Receptor Ablation
883 on Parvalbumin-Positive Interneurons Impairs Hippocampal Synchrony, Spatial Representations, and
884 Working Memory, *Neuron* 68 (3) (2010) 557–569. doi:10.1016/j.neuron.2010.09.017.
885 URL <https://dx.doi.org/10.1016/j.neuron.2010.09.017>
- 886 [31] V. M. Tatard-Leitman, C. R. Jutzeler, J. Suh, J. A. Saunders, E. N. Billingslea, S. Morita, R. White,
887 R. E. Featherstone, R. Ray, P. I. Ortinski, A. Banerjee, M. J. Gandal, R. Lin, A. Alexandrescu,
888 Y. Liang, R. E. Gur, K. E. Borgmann-Winter, G. C. Carlson, C.-G. Hahn, S. J. Siegel, Pyramidal
889 Cell Selective Ablation of N-Methyl-D-Aspartate Receptor 1 Causes Increase in Cellular and Network
890 Excitability, *Biological Psychiatry* 77 (6) (2015) 556–568. doi:10.1016/j.biopsych.2014.06.026.
891 URL <https://dx.doi.org/10.1016/j.biopsych.2014.06.026>
- 892 [32] A. R. Mohn, R. R. Gainetdinov, M. G. Caron, B. H. Koller, Mice with Reduced NMDA Receptor
893 Expression Display Behaviors Related to Schizophrenia, *Cell* 98 (4) (1999) 427–436. doi:10.1016/s0092-
894 8674(00)81972-8.
895 URL [https://dx.doi.org/10.1016/s0092-8674\(00\)81972-8](https://dx.doi.org/10.1016/s0092-8674(00)81972-8)
- 896 [33] A. M. Bygrave, K. Kilonzo, D. M. Kullmann, D. M. Bannerman, D. Kätzel, Can N-Methyl-D-
897 Aspartate Receptor Hypofunction in Schizophrenia Be Localized to an Individual Cell Type?, *Frontiers*
898 *in Psychiatry* 10 (2019) 835–835. doi:10.3389/fpsy.2019.00835.
899 URL <https://dx.doi.org/10.3389/fpsy.2019.00835>
- 900 [34] C. Mayer, C. Hafemeister, R. C. Bandler, R. Machold, R. B. Brito, X. Jaglin, K. Allaway, A. But-
901 ler, G. Fishell, R. Satija, Developmental diversification of cortical inhibitory interneurons, *Nature*
902 555 (7697) (2018) 457–462. doi:10.1038/nature25999.
903 URL <https://dx.doi.org/10.1038/nature25999>
- 904 [35] R. Priya, M. F. Paredes, T. Karayannis, N. Yusuf, X. Liu, X. Jaglin, I. Graef, A. Alvarez-Buylla,
905 G. Fishell, Activity Regulates Cell Death within Cortical Interneurons through a Calcineurin-
906 Dependent Mechanism, *Cell Reports* 22 (7) (2018) 1695–1709. doi:10.1016/j.celrep.2018.01.007.
907 URL <https://dx.doi.org/10.1016/j.celrep.2018.01.007>
- 908 [36] F. K. Wong, K. Bercsenyi, V. Sreenivasan, A. Portalés, M. Fernández-Otero, O. Marín, Pyramidal
909 cell regulation of interneuron survival sculpts cortical networks, *Nature* 557 (7707) (2018) 668–673.
910 doi:10.1038/s41586-018-0139-6.
- 911 [37] H. Bading, D. Ginty, M. Greenberg, Regulation of gene expression in hippocampal neurons by distinct
912 calcium signaling pathways, *Science* 260 (5105) (1993) 181–186. doi:10.1126/science.8097060.
913 URL <https://dx.doi.org/10.1126/science.8097060>
- 914 [38] H. Bading, M. M. Segal, N. J. Sucher, . H. Dudek, ~. Lipton, S. A. Greenberg, M. E (1995).
- 915 [39] E. L. Yap, M. E. Greenberg, Activity-Regulated Transcription: Bridging the Gap between Neural
916 Activity and Behavior (2018).
917 URL <https://doi.org/10.1016/j.neuron.2018.10.013>
- 918 [40] S. Cull-Candy, S. Brickley, M. Farrant, NMDA receptor subunits: diversity, development and disease,
919 *Current Opinion in Neurobiology* 11 (3) (2001) 327–335. doi:10.1016/s0959-4388(00)00215-4.
920 URL [https://dx.doi.org/10.1016/s0959-4388\(00\)00215-4](https://dx.doi.org/10.1016/s0959-4388(00)00215-4)
- 921 [41] H. Komuro, P. Rakic (1993).
- 922 [42] Q. Xu, M. Tam, S. A. Anderson, Fate mapping Nkx2.1-lineage cells in the mouse telencephalon, *The*
923 *Journal of Comparative Neurology* 506 (1) (2008) 16–29. doi:10.1002/cne.21529.
924 URL <https://dx.doi.org/10.1002/cne.21529>

- 925 [43] K. D. Harris, H. Hochgerner, N. G. Skene, L. Magno, L. Katona, C. B. Gonzales, P. Somogyi,
926 N. Kessaris, S. Linnarsson, J. Hjerling-Leffler, Classes and continua of hippocampal CA1 inhibitory
927 neurons revealed by single-cell transcriptomics, *PLOS Biology* 16 (6) (2018) e2006387–e2006387.
928 doi:10.1371/journal.pbio.2006387.
929 URL <https://dx.doi.org/10.1371/journal.pbio.2006387>
- 930 [44] A. B. Muñoz-Manchado, C. B. Gonzales, A. Zeisel, H. Munguba, B. Bekkouche, N. G. Skene, P. Lön-
931 nerberg, J. Ryge, K. D. Harris, S. Linnarsson, J. Hjerling-Leffler, Diversity of Interneurons in the
932 Dorsal Striatum Revealed by Single-Cell RNA Sequencing and PatchSeq, *Cell Reports* 24 (8) (2018)
933 2179–2190.e7. doi:10.1016/j.celrep.2018.07.053.
934 URL <https://dx.doi.org/10.1016/j.celrep.2018.07.053>
- 935 [45] Y. Tanaka, Y. Tanaka, T. Furuta, Y. Yanagawa, T. Kaneko, The effects of cutting solutions on the
936 viability of GABAergic interneurons in cerebral cortical slices of adult mice, *Journal of Neuroscience*
937 *Methods* 171 (1) (2008) 118–125. doi:10.1016/j.jneumeth.2008.02.021.
938 URL <https://dx.doi.org/10.1016/j.jneumeth.2008.02.021>
- 939 [46] Y. E. Wu, L. Pan, Y. Zuo, X. Li, W. Hong, Detecting Activated Cell Populations Using Single-Cell
940 RNA-Seq, *Neuron* 96 (2017) 1–27.
- 941 [47] A. Butler, P. Hoffman, P. Smibert, E. Papalexi, R. Satija, Integrating single-cell transcriptomic data
942 across different conditions, technologies, and species, *Nature Biotechnology* 36 (5) (2018) 411–420.
943 doi:10.1038/nbt.4096.
944 URL <https://dx.doi.org/10.1038/nbt.4096>
- 945 [48] T. Stuart, A. Butler, P. Hoffman, C. Hafemeister, E. Papalexi, W. M. Mauck, Y. Hao, M. Stoeckius,
946 P. Smibert, R. Satija, Comprehensive Integration of Single-Cell Data. *Cell* (2019).
- 947 [49] A. Paul, M. Crow, R. Raudales, M. He, J. Gillis, Z. J. Huang, Transcriptional Architecture of
948 Synaptic Communication Delineates GABAergic Neuron Identity, *Cell* 171 (3) (2017) 522–539.e20.
949 doi:10.1016/j.cell.2017.08.032.
950 URL <https://dx.doi.org/10.1016/j.cell.2017.08.032>
- 951 [50] B. Tasic, V. Menon, T. N. T. Nguyen, T. T. K. Kim, T. Jarsky, Z. Yao, B. B. Levi, L. T. Gray, S. A.
952 Sorensen, T. Dolbeare, Adult mouse cortical cell taxonomy revealed by single cell transcriptomics,
953 *Nat. Neurosci. advance on* (2016) 1–37.
- 954 [51] B. Tasic, V. Menon, T. N. T. Nguyen, T. T. K. Kim, T. Jarsky, Z. Yao, B. B. Levi, L. T. Gray,
955 S. A. Sorensen, T. Dolbeare, D. Bertagnolli, J. Goldy, N. Shapovalova, S. Parry, C. C. Lee, K. Smith,
956 A. Bernard, L. Madisen, S. M. Sunkin, M. Hawrylycz, C. Koch, H. Zeng, Z. Yao, C. C. Lee, N. Shapo-
957 valova, S. Parry, L. Madisen, S. M. Sunkin, M. Hawrylycz, C. Koch, H. Zeng, Adult mouse cortical cell
958 taxonomy revealed by single cell transcriptomics, *Nature Neuroscience advance on* (January) (2016)
959 1–37. doi:10.1038/nn.4216.
- 960 [52] J. Winterer, D. Lukacsovich, L. Que, A. M. Sartori, W. Luo, C. Földy, Single-cell RNA-Seq charac-
961 terization of anatomically identified OLM interneurons in different transgenic mouse lines, *European*
962 *Journal of Neuroscience* 50 (11) (2019) 3750–3771. doi:10.1111/ejn.14549.
963 URL <https://dx.doi.org/10.1111/ejn.14549>
- 964 [53] B. Tasic, Z. Yao, L. T. Gray, K. A. Smith, T. N. Nguyen, D. Bertagnolli, J. Goldy, E. Garren,
965 M. N. Economo, S. Viswanathan, Shared and distinct transcriptomic cell types across neocortical
966 areas, *Nature* 563 (2018) 72–78.
- 967 [54] E. Favuzzi, R. Deogracias, A. Marques-Smith, P. Maeso, J. Jezequel, D. Exposito-Alonso, M. Balia,
968 T. Kroon, A. J. Hinojosa, E. F. Maraver, B. Rico, Distinct molecular programs regulate synapse speci-
969 ficity in cortical inhibitory circuits, *Science* 363 (6425) (2019) 413–417. doi:10.1126/science.aau8977.
- 970 [55] R. Priya, M. F. Paredes, T. Karayannis, N. Yusuf, X. Liu, X. Jaglin, I. Graef, A. Alvarez-Buylla,
971 G. Fishell, Activity Regulates Cell Death within Cortical Interneurons through a Calcineurin-
972 Dependent Mechanism., *Cell reports* 22 (7) (2018) 1695–1709. doi:10.1016/j.celrep.2018.01.007.
- 973 [56] S. J. Butt, V. H. Sousa, M. V. Fuccillo, J. Hjerling-Leffler, G. Miyoshi, S. Kimura, G. Fishell, The
974 Requirement of Nkx2-1 in the Temporal Specification of Cortical Interneuron Subtypes, *Neuron* 59 (5)
975 (2008) 722–732. doi:10.1016/j.neuron.2008.07.031.

- 976 URL <https://dx.doi.org/10.1016/j.neuron.2008.07.031>
- 977 [57] D. J. Laurie, P. H. Seeburg, Regional and developmental heterogeneity in splicing of the rat brain
978 NMDAR1 mRNA, *The Journal of Neuroscience* 14 (5) (1994) 3180–3194. doi:10.1523/jneurosci.14-
979 05-03180.1994.
- 980 URL <https://dx.doi.org/10.1523/jneurosci.14-05-03180.1994>
- 981 [58] H. Monyer, N. Burnashev, D. J. Laurie, B. Sakmann, P. H. Seeburg, Developmental and regional
982 expression in the rat brain and functional properties of four NMDA receptors, *Neuron* 12 (3) (1994)
983 529–540. doi:10.1016/0896-6273(94)90210-0.
- 984 URL [https://dx.doi.org/10.1016/0896-6273\(94\)90210-0](https://dx.doi.org/10.1016/0896-6273(94)90210-0)
- 985 [59] Z. J. Huang, A. Paul, The diversity of GABAergic neurons and neural communication elements, *Nature*
986 *Reviews Neuroscience* 20 (9) (2019) 563–572. doi:10.1038/s41583-019-0195-4.
- 987 URL <https://dx.doi.org/10.1038/s41583-019-0195-4>
- 988 [60] O. Hobert, I. Carrera, N. Stefanakis, The molecular and gene regulatory signature of a neuron, *Trends*
989 *in Neurosciences* 33 (10) (2010) 435–445. doi:10.1016/j.tins.2010.05.006.
- 990 URL <https://dx.doi.org/10.1016/j.tins.2010.05.006>
- 991 [61] K. Y. Kwan, N. Sestan, E. S. Anton, Transcriptional co-regulation of neuronal migration and laminar
992 identity in the neocortex, *Development* 139 (9) (2012) 1535–1546. doi:10.1242/dev.069963.
- 993 URL <https://dx.doi.org/10.1242/dev.069963>
- 994 [62] R. Janky, A. Verfaillie, H. Imrichová, B. V. de Sande, L. Standaert, V. Christiaens, G. Hulselmans,
995 K. Herten, M. N. Sanchez, D. Potier, D. Svetlichnyy, Z. K. Atak, M. Fiers, J.-C. Marine, S. Aerts,
996 iRegulon: From a Gene List to a Gene Regulatory Network Using Large Motif and Track Collections,
997 *PLoS Computational Biology* 10 (7) (2014) e1003731–e1003731. doi:10.1371/journal.pcbi.1003731.
- 998 URL <https://dx.doi.org/10.1371/journal.pcbi.1003731>
- 999 [63] S. J. Otto, S. R. McCorkle, J. Hover, C. Conaco, J. J. Han, S. Impey, G. S. Yochum, J. J. Dunn, R. H.
1000 Goodman, G. Mandel, A New Binding Motif for the Transcriptional Repressor REST Uncovers Large
1001 Gene Networks Devoted to Neuronal Functions, *Journal of Neuroscience* 27 (25) (2007) 6729–6739.
1002 doi:10.1523/jneurosci.0091-07.2007.
- 1003 URL <https://dx.doi.org/10.1523/jneurosci.0091-07.2007>
- 1004 [64] A. Rodenas-Ruano, A. E. Chávez, M. J. Cossio, P. E. Castillo, R. S. Zukin, REST-dependent epigenetic
1005 remodeling promotes the developmental switch in synaptic NMDA receptors, *Nature Neuroscience*
1006 15 (10) (2012) 1382–1390. doi:10.1038/nn.3214.
- 1007 URL <https://dx.doi.org/10.1038/nn.3214>
- 1008 [65] K. Nikouei, A. B. Muñoz-Manchado, J. Hjerling-Leffler, BCL11B/CTIP2 is highly expressed in
1009 GABAergic interneurons of the mouse somatosensory cortex, *Journal of Chemical Neuroanatomy*
1010 71 (2016) 1–5. doi:10.1016/j.jchemneu.2015.12.004.
- 1011 URL <https://dx.doi.org/10.1016/j.jchemneu.2015.12.004>
- 1012 [66] M. Erburu, I. Muñoz-Cobo, T. Diaz-Perdigon, P. Mellini, T. Suzuki, E. Puerta, R. M.
1013 Tordera, SIRT2 inhibition modulate glutamate and serotonin systems in the prefrontal
1014 cortex and induces antidepressant-like action, *Neuropharmacology* 117 (2017) 195–208.
1015 doi:10.1016/j.neuropharm.2017.01.033.
- 1016 URL <https://dx.doi.org/10.1016/j.neuropharm.2017.01.033>
- 1017 [67] M. Wątroba, D. Szukiewicz, The role of sirtuins in aging and age-related diseases, *Advances in Medical*
1018 *Sciences* 61 (1) (2016) 52–62. doi:10.1016/j.advms.2015.09.003.
- 1019 URL <https://dx.doi.org/10.1016/j.advms.2015.09.003>
- 1020 [68] N. Sharma, E. A. Pollina, M. A. Nagy, E.-L. Yap, F. A. DiBiase, S. Hrvatin, L. Hu, C. Lin, M. E.
1021 Greenberg, ARNT2 Tunes Activity-Dependent Gene Expression through NCoR2-Mediated Repression
1022 and NPAS4-Mediated Activation, *Neuron* 102 (2) (2019) 390–406.e9. doi:10.1016/j.neuron.2019.02.007.
- 1023 URL <https://dx.doi.org/10.1016/j.neuron.2019.02.007>
- 1024 [69] Y. Wu, Y. G. Yao, X. J. Luo, SZDB: A Database for Schizophrenia Genetic Research, *Schizophr. Bull*
1025 43 (2017) 459–471.
- 1026 [70] S. Foundation (2018).

- 1027 [71] A. S. Cristino, S. M. Williams, Z. Hawi, J. Y. An, M. A. Bellgrove, C. E. Schwartz, L. da F Costa,
1028 C. Claudianos, Neurodevelopmental and neuropsychiatric disorders represent an interconnected molec-
1029 ular system, *Molecular Psychiatry* 19 (3) (2014) 294–301. doi:10.1038/mp.2013.16.
1030 URL <https://dx.doi.org/10.1038/mp.2013.16>
- 1031 [72] J. Liu, M. Li, X. J. Luo, B. Su, Systems-level analysis of risk genes reveals the modular nature of
1032 schizophrenia, *Schizophr. Res* 201 (2018) 261–269.
- 1033 [73] K. J. Mitchell, The genetics of neurodevelopmental disease, *Curr. Opin. Neurobiol* 21 (2011) 197–203.
- 1034 [74] Y. Sakai, C. A. Shaw, B. C. Dawson, D. V. Dugas, Z. Al-Mohtaseb, D. E. Hill, H. Y. Zoghbi, Protein
1035 Interactome Reveals Converging Molecular Pathways Among Autism Disorders, *Science Translational*
1036 *Medicine* 3 (86) (2011) 86ra49–86ra49. doi:10.1126/scitranslmed.3002166.
1037 URL <https://dx.doi.org/10.1126/scitranslmed.3002166>
- 1038 [75] E. Favuzzi, R. Deogracias, A. Marques-Smith, P. Maeso, J. Jezequel, D. Exposito-Alonso, M. Balia,
1039 T. Kroon, A. J. Hinojosa, E. F. Maraver, B. Rico, Distinct molecular programs regulate synapse speci-
1040 ficity in cortical inhibitory circuits, *Science* 363 (6425) (2019) 413–417. doi:10.1126/science.aau8977.
1041 URL <https://dx.doi.org/10.1126/science.aau8977>
- 1042 [76] R. Dolmetsch, Excitation-Transcription Coupling: Signaling by Ion Channels to the Nucleus, *Science*
1043 *Signaling* 2003 (166) (2003) pe4–pe4. doi:10.1126/stke.2003.166.pe4.
1044 URL <https://dx.doi.org/10.1126/stke.2003.166.pe4>
- 1045 [77] S. M. Cohen, H. Ma, K. V. Kuchibhotla, B. O. Watson, G. Buzsáki, R. C. Froemke, R. W.
1046 Tsien, Excitation-Transcription Coupling in Parvalbumin-Positive Interneurons Employs a Novel
1047 CaM Kinase-Dependent Pathway Distinct from Excitatory Neurons, *Neuron* 90 (2) (2016) 292–307.
1048 doi:10.1016/j.neuron.2016.03.001.
1049 URL <https://dx.doi.org/10.1016/j.neuron.2016.03.001>
- 1050 [78] N. Flames, R. Pla, D. M. Gelman, J. L. R. Rubenstein, L. Puelles, O. Marin, Delineation of Multiple
1051 Subpallial Progenitor Domains by the Combinatorial Expression of Transcriptional Codes, *Journal of*
1052 *Neuroscience* 27 (36) (2007) 9682–9695. doi:10.1523/jneurosci.2750-07.2007.
1053 URL <https://dx.doi.org/10.1523/jneurosci.2750-07.2007>
- 1054 [79] L. Lim, D. Mi, A. Llorca, O. Marín, Development and Functional Diversification of Cortical Interneu-
1055 rons, *Neuron* 100 (2) (2018) 294–313. doi:10.1016/j.neuron.2018.10.009.
1056 URL <https://dx.doi.org/10.1016/j.neuron.2018.10.009>
- 1057 [80] N. Dehorter, G. Ciceri, G. Bartolini, L. Lim, I. del Pino, O. Marín, Tuning of fast-spiking interneu-
1058 ron properties by an activity-dependent transcriptional switch, *Science* 349 (6253) (2015) 1216–1220.
1059 doi:10.1126/science.aab3415.
1060 URL <https://dx.doi.org/10.1126/science.aab3415>
- 1061 [81] P. Flandin, Y. Zhao, D. Vogt, J. Jeong, J. Long, G. Potter, H. Westphal, J. L. R. Rubenstein, Lhx6 and
1062 Lhx8 Coordinately Induce Neuronal Expression of Shh that Controls the Generation of Interneuron
1063 Progenitors, *Neuron* 70 (5) (2011) 939–950. doi:10.1016/j.neuron.2011.04.020.
1064 URL <https://dx.doi.org/10.1016/j.neuron.2011.04.020>
- 1065 [82] E. L.-L. Pai, D. Vogt, A. Clemente-Perez, G. L. McKinsey, F. S. Cho, J. S. Hu, M. Wimer, A. Paul,
1066 S. F. Darbandi, R. Pla, T. J. Nowakowski, L. V. Goodrich, J. T. Paz, J. L. Rubenstein, Mafk and
1067 c-Maf Have Prenatal Compensatory and Postnatal Antagonistic Roles in Cortical Interneuron Fate
1068 and Function, *Cell Reports* 26 (5) (2019) 1157–1173.e5. doi:10.1016/j.celrep.2019.01.031.
1069 URL <https://dx.doi.org/10.1016/j.celrep.2019.01.031>
- 1070 [83] A. Stanco, R. Pla, D. Vogt, Y. Chen, S. Mandal, J. Walker, R. F. Hunt, S. Lindtner, C. A.
1071 Erdman, A. A. Pieper, S. P. Hamilton, D. Xu, S. C. Baraban, J. L. R. Rubenstein, NPAS1 Re-
1072 presses the Generation of Specific Subtypes of Cortical Interneurons, *Neuron* 84 (5) (2014) 940–953.
1073 doi:10.1016/j.neuron.2014.10.040.
1074 URL <https://dx.doi.org/10.1016/j.neuron.2014.10.040>
- 1075 [84] Z. Liu, Z. Zhang, S. Lindtner, Z. Li, Z. Xu, S. Wei, Q. Liang, Y. Wen, G. Tao, Y. You, Sp9 Regulates
1076 Medial Ganglionic Eminence-Derived Cortical Interneuron Development, *Cereb. Cortex* (2018) 1–15.
- 1077 [85] R. D. Hodge, T. E. Bakken, J. A. Miller, K. A. Smith, E. R. Barkan, L. T. Graybuck, J. L. Close,

- 1078 B. Long, N. Johansen, O. Penn, Conserved cell types with divergent features in human versus mouse
1079 cortex, *Nature* (2019).
- 1080 [86] Z. Yao, T. N. Nguyen, C. T. J. Velthoven, Van, J. Goldy, A. E. Seden-Cortes, F. Baftizadeh,
1081 D. Bertagnolli, T. Casper, K. Crichton, S. L. Ding (2020).
- 1082 [87] G. Fishell, A. Kepecs, Interneuron Types as Attractors and Controllers (2020). doi:10.1146/annurev-
1083 neuro-070918-050421.
1084 URL <https://dx.doi.org/10.1146/annurev-neuro-070918-050421>
- 1085 [88] W. Andrews, M. Barber, L. R. Hernandez-Miranda, J. Xian, S. Rakic, V. Sundaresan, T. H. Rabbitts,
1086 R. Pannell, P. Rabbitts, H. Thompson, L. Erskine, F. Murakami, J. G. Parnavelas, The role of Slit-
1087 Robo signaling in the generation, migration and morphological differentiation of cortical interneurons,
1088 *Developmental Biology* 313 (2) (2008) 648–658. doi:10.1016/j.ydbio.2007.10.052.
1089 URL <https://dx.doi.org/10.1016/j.ydbio.2007.10.052>
- 1090 [89] F. Polleux, K. L. Whitford, P. A. Dijkhuizen, T. Vitalis, A. Ghosh, Control of cortical interneuron
1091 migration by neurotrophins and PI3-kinase signaling, *Development* 129 (2002) 3147–3160.
- 1092 [90] O. Marín, A. Yaron, A. Bagri, M. Tessier-Lavigne, J. L. R. Rubenstein, Sorting of Striatal and Cortical
1093 Interneurons Regulated by Semaphorin-Neuropilin Interactions, *Science* 293 (2001) 872–875.
- 1094 [91] S. Nobrega-Pereira, O. Marín, Transcriptional Control of Neuronal Migration in the Developing Mouse
1095 Brain, *Cerebral Cortex* 19 (suppl 1) (2009) i107–i113. doi:10.1093/cercor/bhp044.
1096 URL <https://dx.doi.org/10.1093/cercor/bhp044>
- 1097 [92] S. Nóbrega-Pereira, N. Kessar, T. Du, S. Kimura, S. A. Anderson, O. Marín, Postmitotic Nkx2-1
1098 Controls the Migration of Telencephalic Interneurons by Direct Repression of Guidance Receptors,
1099 *Neuron* 59 (5) (2008) 733–745. doi:10.1016/j.neuron.2008.07.024.
1100 URL <https://dx.doi.org/10.1016/j.neuron.2008.07.024>
- 1101 [93] A. Stancu, C. Szekeres, N. Patel, S. Rao, K. Campbell, J. A. Kreidberg, F. Polleux, E. S. An-
1102 ton, Netrin-1- 3 1 integrin interactions regulate the migration of interneurons through the corti-
1103 cal marginal zone, *Proceedings of the National Academy of Sciences* 106 (18) (2009) 7595–7600.
1104 doi:10.1073/pnas.0811343106.
1105 URL <https://dx.doi.org/10.1073/pnas.0811343106>
- 1106 [94] A. Steinecke, C. Gampe, G. Zimmer, J. Rudolph, J. Bolz, EphA/ephrin A reverse signaling promotes
1107 the migration of cortical interneurons from the medial ganglionic eminence, *Development* 141 (2)
1108 (2014) 460–471. doi:10.1242/dev.101691.
1109 URL <https://dx.doi.org/10.1242/dev.101691>
- 1110 [95] G. Zimmer, P. Garcez, J. Rudolph, R. Niehage, F. Weth, R. Lent, J. Bolz, Ephrin-A5 acts as a
1111 repulsive cue for migrating cortical interneurons, *European Journal of Neuroscience* 28 (1) (2008)
1112 62–73. doi:10.1111/j.1460-9568.2008.06320.x.
1113 URL <https://dx.doi.org/10.1111/j.1460-9568.2008.06320.x>
- 1114 [96] Z. Shao, H. Noh, W. B. Kim, P. Ni, C. Nguyen, S. E. Cote, E. Noyes, J. Zhao, T. Parsons, J. M.
1115 Park, Dysregulated protocadherin-pathway activity as an intrinsic defect in induced pluripotent stem
1116 cell-derived cortical interneurons from subjects with schizophrenia, *Nat. Neurosci* 22 (2019) 229–242.
- 1117 [97] B. L. Bloodgood, N. Sharma, H. A. Browne, A. Z. Trepman, M. E. Greenberg, The activity-dependent
1118 transcription factor NPAS4 regulates domain-specific inhibition, *Nature* 503 (7474) (2013) 121–125.
1119 doi:10.1038/nature12743.
1120 URL <https://dx.doi.org/10.1038/nature12743>
- 1121 [98] Y. Lin, B. L. Bloodgood, J. L. Hauser, A. D. Lapan, A. C. Koon, T.-K. Kim, L. S. Hu, A. N. Malik,
1122 M. E. Greenberg, Activity-dependent regulation of inhibitory synapse development by Npas4, *Nature*
1123 455 (7217) (2008) 1198–1204. doi:10.1038/nature07319.
1124 URL <https://dx.doi.org/10.1038/nature07319>
- 1125 [99] X. Sun, Lin, Y, Npas4: Linking Neuronal Activity to Memory, *Trends Neurosci* 39 (2016) 264–275.
- 1126 [100] I. Spiegel, A. R. Mardinly, H. W. Gabel, J. E. Bazinet, C. H. Couch, C. P. Tzeng, D. A. Harmin, M. E.
1127 Greenberg, Npas4 Regulates Excitatory-Inhibitory Balance within Neural Circuits through Cell-Type-
1128 Specific Gene Programs, *Cell* 157 (5) (2014) 1216–1229. doi:10.1016/j.cell.2014.03.058.

- 1129 URL <https://dx.doi.org/10.1016/j.cell.2014.03.058>
- 1130 [101] B. Ataman, G. L. Boulting, D. A. Harmin, M. G. Yang, M. Baker-Salisbury, E.-L. Yap, A. N. Malik,
1131 K. Mei, A. A. Rubin, I. Spiegel, E. Durrezi, N. Sharma, L. S. Hu, M. Pletikos, E. C. Griffith, J. N.
1132 Partlow, C. R. Stevens, M. Adli, M. Chahrour, N. Sestan, C. A. Walsh, V. K. Berezovskii, M. S.
1133 Livingstone, M. E. Greenberg, Evolution of Osteocrin as an activity-regulated factor in the primate
1134 brain, *Nature* 539 (7628) (2016) 242–247. doi:10.1038/nature20111.
1135 URL <https://dx.doi.org/10.1038/nature20111>
- 1136 [102] B. Lacar, S. B. Linker, B. N. Jaeger, S. R. Krishnaswami, J. J. Barron, M. J. E. Kelder, S. L. Parylak,
1137 A. C. M. Paquola, P. Venepally, M. Novotny, Nuclear RNA-seq of single neurons reveals molecular
1138 signatures of activation, *Nat. Commun* 7 (2016) 11022–11022.
- 1139 [103] C. M. Müller, A. Vlachos, T. Deller, Calcium homeostasis of acutely denervated and lesioned den-
1140 tate gyrus in organotypic entorhino-hippocampal co-cultures, *Cell Calcium* 47 (3) (2010) 242–252.
1141 doi:10.1016/j.ceca.2009.12.006.
1142 URL <https://dx.doi.org/10.1016/j.ceca.2009.12.006>
- 1143 [104] W. XiangWei, Y. Jiang, H. Yuan, De novo mutations and rare variants occurring in NMDA receptors,
1144 *Current Opinion in Physiology* 2 (2018) 27–35. doi:10.1016/j.cophys.2017.12.013.
1145 URL <https://dx.doi.org/10.1016/j.cophys.2017.12.013>
- 1146 [105] J. C. Masdeu, J. Dalmau, K. F. Berman, NMDA Receptor Internalization by Autoantibodies:
1147 A Reversible Mechanism Underlying Psychosis?, *Trends in Neurosciences* 39 (5) (2016) 300–310.
1148 doi:10.1016/j.tins.2016.02.006.
1149 URL <https://dx.doi.org/10.1016/j.tins.2016.02.006>
- 1150 [106] J. Tarabeux, , O. Kebir, J. Gauthier, F. F. Hamdan, L. Xiong, A. Piton, D. Spiegelman, E. Henrion,
1151 B. Millet, F. Fathalli, R. Joobor, J. L. Rapoport, L. E. DeLisi, E. Fombonne, L. Mottron, N. Forget-
1152 Dubois, M. Boivin, J. L. Michaud, P. Drapeau, R. G. Lafrenière, G. A. Rouleau, M. O. Krebs, Rare
1153 mutations in N-methyl-D-aspartate glutamate receptors in autism spectrum disorders and schizophre-
1154 nia, *Translational Psychiatry* 1 (11) (2011) e55–e55. doi:10.1038/tp.2011.52.
1155 URL <https://dx.doi.org/10.1038/tp.2011.52>
- 1156 [107] Y. Yu, Y. Lin, Y. Takasaki, C. Wang, H. Kimura, J. Xing, K. Ishizuka, M. Toyama, I. Kushima,
1157 D. Mori, Rare loss of function mutations in N-methyl-d-aspartate glutamate receptors and their con-
1158 tributions to schizophrenia susceptibility, *Transl. Psychiatry* 8 (2018) 12–12.
- 1159 [108] W. Chen, C. Shieh, S. A. Swanger, A. Tankovic, M. Au, M. McGuire, M. Tagliati, J. M. Graham,
1160 S. Madan-Khetarpal, S. F. Traynelis, H. Yuan, T. M. Pierson, GRIN1 mutation associated with
1161 intellectual disability alters NMDA receptor trafficking and function, *Journal of Human Genetics*
1162 62 (6) (2017) 589–597. doi:10.1038/jhg.2017.19.
1163 URL <https://dx.doi.org/10.1038/jhg.2017.19>
- 1164 [109] L. L. Gibson, T. A. Pollak, G. Blackman, M. Thornton, N. Moran, A. S. David, The Psychiatric
1165 Phenotype of Anti-NMDA Receptor Encephalitis, *The Journal of Neuropsychiatry and Clinical Neu-*
1166 *rosciences* 31 (1) (2019) 70–79. doi:10.1176/appi.neuropsych.17120343.
1167 URL <https://dx.doi.org/10.1176/appi.neuropsych.17120343>
- 1168 [110] G. L. Carvill, B. M. Regan, S. C. Yendle, B. J. O’Roak, N. Lozovaya, N. Bruneau, N. Burnashev,
1169 A. Khan, J. Cook, E. Geraghty, L. G. Sadleir, S. J. Turner, M.-H. Tsai, R. Webster, R. Ouvrier, J. A.
1170 Damiano, S. F. Berkovic, J. Shendure, M. S. Hildebrand, P. Szepetowski, I. E. Scheffer, H. C. Mefford,
1171 GRIN2A mutations cause epilepsy-aphasia spectrum disorders, *Nature Genetics* 45 (9) (2013) 1073–
1172 1076. doi:10.1038/ng.2727.
1173 URL <https://dx.doi.org/10.1038/ng.2727>
- 1174 [111] J. R. Lemke, D. Lal, E. M. Reinthaler, I. Steiner, M. Nothnagel, M. Alber, K. Geider, B. Laube,
1175 M. Schwake, K. Finsterwalder, Mutations in GRIN2A cause idiopathic focal epilepsy with rolandic
1176 spikes, *Nat. Genet* 45 (2013) 1067–1072.
- 1177 [112] S. J. Dienel, D. A. Lewis, Alterations in cortical interneurons and cognitive function in schizophrenia,
1178 *Neurobiology of Disease* 131 (2019) 104208–104208. doi:10.1016/j.nbd.2018.06.020.
1179 URL <https://dx.doi.org/10.1016/j.nbd.2018.06.020>

- 1180 [113] D. A. Lewis, T. Hashimoto, D. W. Volk, Cortical inhibitory neurons and schizophrenia, *Nature Reviews*
1181 *Neuroscience* 6 (4) (2005) 312–324. doi:10.1038/nrn1648.
1182 URL <https://dx.doi.org/10.1038/nrn1648>
- 1183 [114] F. Ali, D. M. Gerhard, K. Sweasy, S. Pothula, C. Pittenger, R. S. Duman, A. C. Kwan, Ketamine
1184 disinhibits dendrites and enhances calcium signals in prefrontal dendritic spines, *Nature Communica-*
1185 *tions* 11 (1) (2020) 72–72. doi:10.1038/s41467-019-13809-8.
1186 URL <https://dx.doi.org/10.1038/s41467-019-13809-8>
- 1187 [115] R. Chittajallu, K. Auville, V. Mahadevan, M. Lai, S. Hunt, D. Calvigioni, K. A. Pelkey, K. Zaghloul,
1188 C. J. Mcbain (2020).
- 1189 [116] K. Nakao, V. Jeevakumar, S. Z. Jiang, Y. Fujita, N. B. Diaz, C. A. P. Annan, K. L. E. Jaunaraajs,
1190 K. Hashimoto, J. E. Belforte, K. Nakazawa (2018).
- 1191 [117] R. C. Team (2013).
- 1192 [118] A. Paul, M. Crow, R. Raudales, J. Gillis, Z. J. Huang, Transcriptional Architecture of Synap-
1193 tic Communication Delineates Cortical GABAergic Neuron Identity, *Cell* 171 (3) (2017) 522–539.
1194 doi:10.1016/j.cell.2017.08.032.
- 1195 [119] A. Saunders, E. Z. Macosko, A. Wysoker, M. Goldman, F. M. Krienen, H. de Rivera, E. Bien, M. Baum,
1196 L. Bortolin, S. Wang, A. Goeva, J. Nimesh, N. Kamitaki, S. Brumbaugh, D. Kulp, S. A. McCarroll,
1197 Molecular Diversity and Specializations among the Cells of the Adult Mouse Brain, *Cell* 174 (4) (2018)
1198 1015–1030.e16. doi:10.1016/j.cell.2018.07.028.
1199 URL <https://dx.doi.org/10.1016/j.cell.2018.07.028>
- 1200 [120] Z. Yao, T. N. Nguyen, C. T. J. van Velthoven, J. Goldy, A. E. Seden-Cortes, F. Baftizadeh, D. Bertag-
1201 nonli, T. Casper, K. Crichton, S.-L. Ding, O. Fong, E. Garren, A. Glandon, J. Gray, L. T. Graybuck,
1202 D. Hirschstein, M. Kroll, K. Lathia, B. Levi, D. McMillen, S. Mok, T. Pham, Q. Ren, C. Rimorin,
1203 N. Shapovalova, J. Sulc, S. M. Sunkin, M. Tieu, A. Torkelson, H. Tung, K. Ward, N. Dee, K. A.
1204 Smith, B. Tasic, H. Zeng, A taxonomy of transcriptomic cell types across the isocortex and hippocam-
1205 pal formation, *bioRxiv* (mar 2020). doi:10.1101/2020.03.30.015214.
- 1206 [121] G. Finak, A. McDavid, M. Yajima, J. Deng, V. Gersuk, A. K. Shalek, C. K. Slichter, H. W. Miller,
1207 M. J. McElrath, M. Pric, P. S. Linsley, R. Gottardo, MAST: a flexible statistical framework for
1208 assessing transcriptional changes and characterizing heterogeneity in single-cell RNA sequencing data,
1209 *Genome Biology* 16 (1) (2015). doi:10.1186/s13059-015-0844-5.
1210 URL <https://dx.doi.org/10.1186/s13059-015-0844-5>
- 1211 [122] M. Ximerakis, S. L. Lipnick, B. T. Innes, S. K. Simmons, X. Adiconis, D. Dionne, B. A. Mayweather,
1212 L. Nguyen, Z. Niziolek, C. Ozek, V. L. Butty, R. Isserlin, S. M. Buchanan, S. S. Levine, A. Regev,
1213 G. D. Bader, J. Z. Levin, L. L. Rubin, Single-cell transcriptomic profiling of the aging mouse brain,
1214 *Nature Neuroscience* 22 (10) (2019) 1696–1708. doi:10.1038/s41593-019-0491-3.
1215 URL <https://dx.doi.org/10.1038/s41593-019-0491-3>
- 1216 [123] B. Kevin (2019). [link].
1217 URL <https://Github.Com/Kevinblighe/EnhancedVolcano>
- 1218 [124] S. X. Ge, D. Jung, R. Yao, ShinyGO: a graphical gene-set enrichment tool for animals and plants,
1219 *Bioinformatics* 36 (8) (2020) 2628–2629. doi:10.1093/bioinformatics/btz931.
1220 URL <https://dx.doi.org/10.1093/bioinformatics/btz931>
- 1221 [125] K. R. Brown, I. Jurisica, Unequal evolutionary conservation of human protein interactions in interol-
1222 ogous networks, *Genome Biology* 8 (5) (2007) R95–R95. doi:10.1186/gb-2007-8-5-r95.
1223 URL <https://dx.doi.org/10.1186/gb-2007-8-5-r95>
- 1224 [126] M. Kotlyar, C. Pastrello, F. Pivetta, A. L. Sardo, C. Cumbaa, H. Li, T. Naranian, Y. Niu, Z. Ding,
1225 F. Vafae, F. Broackes-Carter, J. Petschnigg, G. B. Mills, A. Jurisicova, I. Stagljar, R. Maestro,
1226 I. Jurisica, In silico prediction of physical protein interactions and characterization of interactome
1227 orphans, *Nature Methods* 12 (1) (2015) 79–84. doi:10.1038/nmeth.3178.
1228 URL <https://dx.doi.org/10.1038/nmeth.3178>
- 1229 [127] C. Stark, BioGRID: a general repository for interaction datasets, *Nucleic Acids Research* 34 (90001)
1230 (2006) D535–D539. doi:10.1093/nar/gkj109.

- 1231 URL <https://dx.doi.org/10.1093/nar/gkj109>
- 1232 [128] V. Mahadevan, C. S. Khademullah, Z. Dargaei, J. Chevrier, P. Uvarov, J. Kwan, R. D. Bagshaw,
1233 T. Pawson, A. Emili, Y. D. Koninck (2017).
- 1234 [129] M. E. Smoot, K. Ono, J. Ruscheinski, P. L. Wang, T. Ideker, Cytoscape 2.8: new fea-
1235 tures for data integration and network visualization, *Bioinformatics* 27 (3) (2011) 431–432.
1236 doi:10.1093/bioinformatics/btq675.
1237 URL <https://dx.doi.org/10.1093/bioinformatics/btq675>